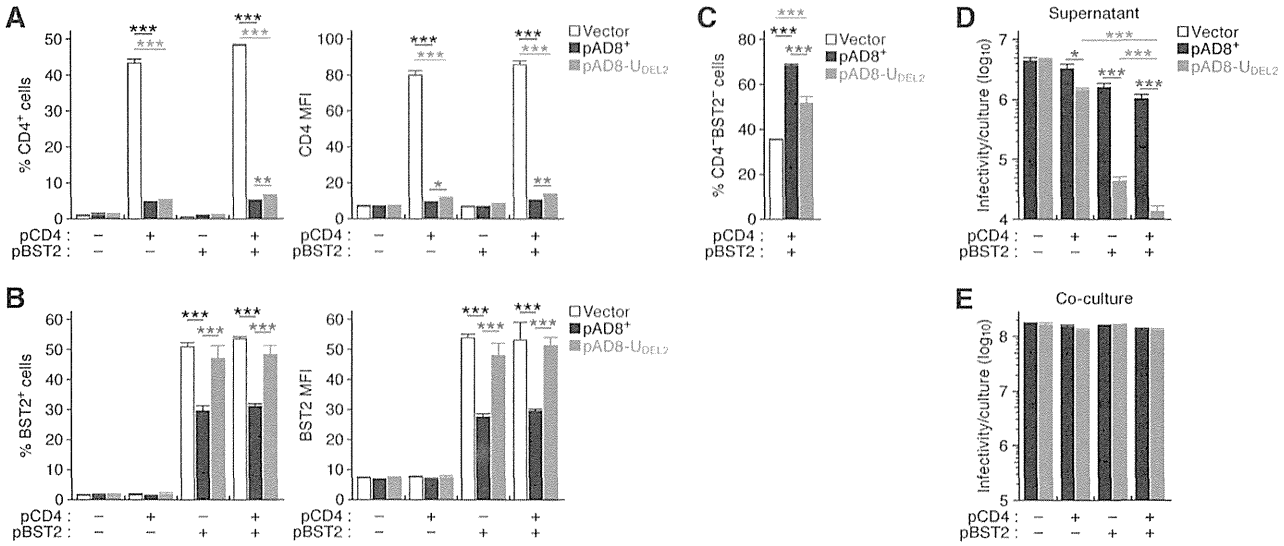

FIG 9 Different potentials of CD4 and BST2 in the production of infectious cell-free virions and cell-to-cell HIV-1 transmission. A total of 800 ng of pAD8$^+$ (WT HIV-1-producing plasmid), pAD8-U$_{DEL2}$ (*vpu*-deficient HIV-1-producing plasmid), or pUC19 (parental plasmid; vector) was cotransfected with either 10 ng of CD4 expression plasmid (pCD4) or BST2 expression plasmid (pBST2) or both into HEK293 cells. peGFP-C1 (100 ng) was also cotransfected to monitor transfection efficiency. The assay was performed in quadruplicate. (A to C) Downregulation of surface CD4 and BST2. The surface expression levels of CD4 and BST2 on the transfected HEK293 cells (i.e., GFP-positive cells) at 48 h posttransfection were assessed by flow cytometry. The positive percentage (left) and the MFI (right) are shown. The percentage of the cells negative for both CD4 and BST2 in the cells cotransfected with both pCD4 and pBST2 is also shown (C). (D and E) Infectious potentials of cell-free virions in culture supernatant and transfected cells. The infectivities of the viruses in the supernatant and the transfected cells (coculture) were titrated by TZM-bl assay and were normalized to the values per culture. Statistically significant differences (determined by Student's *t* test) are shown as follows: *, $P < 0.05$; **, $P < 0.01$; ***, $P < 0.001$. Error bars represent SEMs.

and BST2 do not have the potential to attenuate cell-to-cell HIV-1 infection and that Vpu slightly associates with the efficiency of cell-to-cell viral transmission.

DISCUSSION

The significance of Vpu for HIV-1 infection, especially in terms of its interplay with BST2, has been extensively investigated in cell culture experiments. However, its importance for HIV-1 propagation *in vivo* remains unclear and needs to be addressed (7, 26). In this study, we used *vpu*-deficient CCR5-tropic HIV-1 to infect a humanized mouse model, which allowed us to track the pathogenesis of HIV-1 from the onset of infection, and elucidated the role of Vpu in HIV-1 propagation *in vivo*. Our results demonstrate that Vpu downregulates CD4 and BST2 on the surface of infected cells and enhances viral dissemination during the initial phase of infection *in vivo*. This is the first report directly implicating the importance of Vpu during HIV-1 infection *in vivo*.

Although our findings suggest that Vpu is weakly associated with the viral cytotoxicity of HIV-1 infection *in vivo*, we hypothesize that its involvement in early viral replication kinetics may be critical. In our humanized mouse model, the preference of target cells (Fig. 3B and C), the level of viral protein expression (Fig. 4D), and the cytopathic effect (Fig. 2C to F) were nearly identical between WT and *vpu*-deficient HIV-1-infected mice. However, the kinetics of early viral expansion in WT HIV-1-infected mice was significantly higher than in HIV-1Δ*vpu*-infected mice (Fig. 2B). In addition, although the percentage of Gag-positive cells in the spleen of WT HIV-1-infected mice at 7 dpi was only 2.8-fold higher than that of HIV-1Δ*vpu*-infected mice (Fig. 4B), the amount of cell-free virions in WT HIV-1-infected spleens was 38.2-fold higher (Fig. 4A). Moreover, the levels of cell-free virions positively and significantly correlated with infected cells in the spleen of WT HIV-1-infected mice but not in HIV-1Δ*vpu*-infected mice (Fig. 4C). Interestingly, significant downregulation of BST2 by WT HIV-1 appeared to be important for this virus dissemination to occur (Fig. 5B). Taken together, our findings suggest that the Vpu antagonism of BST2 closely associates with the efficiency of virus expansion *in vivo*, especially during the early phase of infection.

The amount of cell-free virions in the spleen of WT HIV-1-infected mice was prominently (38.2-fold) higher than that in HIV-1Δ*vpu*-infected mice (Fig. 4A); however, statistical significance was not determined. To obtain the specimens of cell suspensions and cell-free virions from the spleen of infected mice, the spleen was mechanically dissociated according to a conventional method. In carrying out this procedure, it is possible that the virions tethered by BST2 on the surface of HIV-1Δ*vpu*-infected cells were partially dissociated. In fact, one study has suggested that the virions tethered by BST2 can be partially dissociated by mechanical agitation using a vortex (38). Therefore, it might be possible to assume that the virions tethered by BST2 on the surface of *vpu*-deficient HIV-1-infected cells partially dissociated by our procedure, which led to no statistical difference.

In comparing the level of Gag expression in HIV-1-infected cells, we noticed differences depending on the method used for detection. Flow cytometry analyses of Pr55^{Gag} expression in *vpu*-deficient HIV-1-producing cells produced results comparable to those in WT HIV-1-producing cells in the transfected HeLa cells (data not shown), infected primary human CD4$^+$ T cells (data not shown), and infected humanized mice (Fig. 4D), suggesting equal levels of virus production. On the other hand, Western blotting

analyses revealed that the amount of p24 in the pAD8-U_{DEL2}-transfected HeLa cells was clearly higher than that in the pAD8$^+$-transfected HeLa cells (Fig. 1B) although the expression levels of $Pr55^{Gag}$ were equal (Fig. 1B). These data indicate that the release of virions in the absence of Vpu was impaired. HIV-1 particles tethered on the plasma membrane are rapidly endocytosed and accumulate in endosomal compartments (40). Thus, the anti-p24 antibody used for flow cytometry may have underestimated the total amount of Gag proteins because only intracellular $Pr55^{Gag}$ was detected as p24 of virions in the endosomal compartment was not accessible.

As shown in Fig. 2B, HIV-1 propagated more rapidly in humanized mice at the highest dose than at the other doses. These results suggest that the kinetics of viral growth is dependent on the dose of inoculated viruses. On the other hand, the cytopathic effect was observed in the PB of infected mice at 14 and 21 dpi at the highest dose but not at the other doses (Fig. 2C to E). In this regard, we have previously observed that the viral load of HIV-1-infected humanized mice reached a plateau at 3 to 4 weeks postinfection and that peripheral CD4$^+$ T cells, especially memory CD4$^+$ T cells, in infected humanized mice gradually decreased at later time points (after 9 weeks postinfection) (44, 52). Therefore, it is conceivable that the cytopathic effect (i.e., the decrease of peripheral CD4$^+$ T cells) in infected mice at the highest dose at 14 and 21 dpi (Fig. 2C and D) is caused by faster viral dissemination than at the other doses and that the cytopathic effect would be observed at later time points in infected mice at lower doses.

It was reported that CD4, BST2, and SLAMF6 are downregulated from the surface of HIV-1-infected cells by Vpu in cell culture systems (7, 9, 31, 64). Here, we demonstrated that the Vpu encoded by strain AD8 is able to downregulate these three molecules from the surface of infected cells *in vitro* (Fig. 1D to F). However, the magnitude of Vpu-mediated downregulation of each cellular protein *in vivo* remains unknown. We observed that CD4 and BST2 were significantly downregulated by Vpu expressed in infected cells at both 7 dpi (Fig. 5) and 21 dpi (Fig. 7). We also demonstrated that both molecules were downregulated from the surface of the same infected cells in a Vpu-dependent manner (Fig. 6). In contrast to CD4 and BST2, Vpu-dependent SLAMF6 downregulation was not observed in infected humanized mice (Fig. 5C and 6C). Therefore, our results suggest that Vpu downregulates cell surface CD4 and BST2 both *in vitro* and *in vivo*, while that the sequestration of SLAMF6 from the surface of infected cells is not sufficiently elicited by Vpu *in vivo*.

It has been reported that CD4 expressed on the surface of infected cells has the potential to impair HIV-1 replication by (i) inhibiting the release of progeny virions (48), (ii) impairing the incorporation of Env into nascent virions (6, 29), and (iii) sequestering Env from the virion budding site (3, 6, 29, 31, 32). We confirmed that CD4 suppresses the production of infectious virions (Fig. 9D). Moreover, we provide the first evidence demonstrating that CD4 and BST2 synergistically suppress the production of infectious virions (Fig. 9D). Therefore, in accordance with previous reports (29, 31), our results suggest that not only BST2 but also CD4 possesses the potential to impair the production of infectious nascent virions, which can be counteracted by Vpu.

Even though Vpu downregulated CD4 and BST2 at 21 dpi (Fig. 7), the levels of plasma viral load and splenic cell-free virion in *vpu*-deficient HIV-1-infected mice became equal to those in WT HIV-1-infected mice (Fig. 2B and 3A). These findings raise the possibility that *vpu*-deficient HIV-1 is able to overcome the restriction mediated by CD4 and BST2 at this point. Interestingly, it has been reported that HIV-1 can be transmitted through cell-to-cell contact (17–22, 36, 57). In addition, although it is still controversial (5, 28), one study has recently demonstrated that the cell-to-cell HIV-1 spread is not restricted by BST2 in a T cell culture system (16). By using an *in vitro* transfection system, we demonstrated that CD4 and BST2 did not associate with cell-to-cell infection and that the efficiency of cell-to-cell transmission was not enhanced by Vpu (Fig. 9E). Moreover, we found that the majority of Gag-positive cells in the spleens of WT and *vpu*-deficient HIV-1-infected mice were in contact with each other (Fig. 8). Taken together, our findings, in agreement with previous reports, strongly suggest that cell-to-cell virus transmission efficiently occurs in humanized mice at 21 dpi and is not restricted by BST2 and CD4.

As mentioned above, viruses are propagated by two modes: cell-free virus-mediated transmission and cell-to-cell transmission. In comparisons of these two modes of transmission, it has been reported that cell-to-cell HIV-1 spread is more efficient than cell-free infection in *in vitro* cell culture systems (4, 50). Here, we found that the infectivity of transfected cells per culture was markedly higher than that of the supernatant per culture (Fig. 9D and E). Given that leukocytes, including CD4$^+$ T cells, exist in dense clumps and are in contact with each other in lymphoid tissues (e.g., spleen), it is feasible to assume that HIV-1 dissemination is more likely to occur through cell-to-cell contact *in vivo*. Moreover, previous reports have demonstrated that BST2 potently impairs the release of *Orthomyxoviridae* (influenza A virus) and *Filoviridae* (Ebola virus and Marburg virus); however, BST2 does not suppress the spread of these viruses in *in vitro* cell cultures (47, 69). Therefore, it is conceivable that BST2 does not impair the cell-to-cell spread of viruses even if the cell-free virus-mediated infection of these viruses is restricted by BST2.

Andrew and Strebel have recently suggested that endogenous BST2 is not a "restrictive factor" that limits HIV-1 spread but, rather, a "modulator" that shifts the mode of HIV-1 infection from cell-free spread to cell-to-cell transmission (2). Building upon this hypothesis, we used our current findings, together with previous reports, to propose a model regarding the role of Vpu in HIV-1 infection *in vivo*. During the acute phase of infection (until 7 dpi in humanized mice), when the level of infected cells in the body is low (Fig. 4B), cell-free virus-mediated infection serves as the major route of virus spread *in vivo*. Therefore, Vpu-mediated counteraction of BST2 (and CD4) has a crucial role for the efficient virus amplification *in vivo* during this phase. From our data, the reduced infectivity of *vpu*-deficient HIV-1 compared to WT HIV-1 in humanized mice (Fig. 2A) further suggests the importance of a boost in the amount of cell-free viruses necessary for the establishment of virus production *in vivo*. However, at a later stage of infection when the level of infected cells achieves a certain threshold (21 dpi in humanized mice), HIV-1 would be mainly propagated through cell-to-cell transmission, which is resistant to BST2-mediated restriction. Therefore, the antagonistic behavior of Vpu would become dispensable for efficient virus spread at this point. In summary, consistent with the concept proposed by Andrew and Strebel (2), our findings suggest that endogenous BST2 is not a restrictive but a modulatory factor for HIV-1 spread *in vivo*.

ACKNOWLEDGMENTS

We thank Peter Gee (Laboratory of Viral Pathogenesis, Institute for Virus Research, Kyoto University) for proofreading the manuscript, and Takao Ueno (Graduate School of Mathematical Sciences, the University of Tokyo), Mariko Horiike (Institute for Virus Research, Kyoto University), Takashi Nakano, and Kouichi Sano (Osaka Medical College) for their generous help in our study. We also thank Klaus Strebel (National Institute of Allergy and Infectious Diseases, National Institutes of Health) for providing HIV-1-producing plasmids (pAD8^{+} and pAD8-U_{DEL2}) and a rabbit anti-Vpu polyclonal antibody (U2-3), Yuetsu Tanaka (University of the Ryukyus) for providing a rat anti-p24 monoclonal antibody (clone 2C2), and Masayuki Miyasaka (Osaka University Graduate School of Medicine) for providing a human CD4 expression plasmid (pBCMGSNeo-human CD4). We appreciate Kotubu Misawa's dedicated support.

This work was supported in part by grants from the following: Grants-in-Aid for Scientific Research B21390137 (to Y.K.) and S22220007 (to M.I. and Y.K.) and a Grant-in-Aid for Young Scientists B23790500 (to K.S.) from the Japan Society for the Promotion of Science; grants from Research on Emerging and Reemerging Infectious Diseases (to Y.K.) and Research on HIV/AIDS (to Y.K.) from the Ministry of Health, Labor and Welfare of Japan; a grant from the Uehara Memorial Foundation (to K.S.); JST PRESTO program (to S.I.); and a UCLA CFAR grant 5P30AI028697 (to D.S.A).

REFERENCES

1. **An DS, et al.** 2007. Use of a novel chimeric mouse model with a functionally active human immune system to study human immunodeficiency virus type 1 infection. Clin. Vaccine Immunol. 14:391–396.
2. **Andrew A, Strebel K.** 2011. The interferon-inducible host factor bone marrow stromal antigen 2/tetherin restricts virion release, but is it actually a viral restriction factor? J. Interferon Cytokine Res. 31:137–144.
3. **Arganaraz ER, Schindler M, Kirchhoff F, Cortes MJ, Lama J.** 2003. Enhanced CD4 down-modulation by late stage HIV-1 *nef* alleles is associated with increased Env incorporation and viral replication. J. Biol. Chem. 278:33912–33919.
4. **Carr JM, Hocking H, Li P, Burrell CJ.** 1999. Rapid and efficient cell-to-cell transmission of human immunodeficiency virus infection from monocyte-derived macrophages to peripheral blood lymphocytes. Virology 265:319–329.
5. **Casartelli N, et al.** 2010. Tetherin restricts productive HIV-1 cell-to-cell transmission. PLoS Pathog. 6:e1000955.
6. **Cortes MJ, Wong-Staal F, Lama J.** 2002. Cell surface CD4 interferes with the infectivity of HIV-1 particles released from T cells. J. Biol. Chem. 277:1770–1779.
7. **Douglas JL, et al.** 2010. The great escape: viral strategies to counter BST-2/tetherin. PLoS Pathog. 6:e1000913.
8. **Douglas JL, et al.** 2009. Vpu directs the degradation of the human immunodeficiency virus restriction factor BST-2/tetherin via a βTrCP-dependent mechanism. J. Virol. 83:7931–7947.
9. **Evans DT, Serra-Moreno R, Singh RK, Guatelli JC.** 2010. BST-2/tetherin: a new component of the innate immune response to enveloped viruses. Trends Microbiol. 18:388–396.
10. **Freed EO, Martin MA.** 2007. HIVs and their replication, p 2107–2185. *In* Knipe DM, et al (ed), Fields virology, 5th ed, vol 2. Lippincott Williams & Wilkins, Philadelphia, PA.
11. **Goffinet C, et al.** 2009. HIV-1 antagonism of CD317 is species specific and involves Vpu-mediated proteasomal degradation of the restriction factor. Cell Host Microbe 5:285–297.
12. **Gottlinger HG, Dorfman T, Cohen EA, Haseltine WA.** 1993. Vpu protein of human immunodeficiency virus type 1 enhances the release of capsids produced by gag gene constructs of widely divergent retroviruses. Proc. Natl. Acad. Sci. U. S. A. 90:7381–7385.
13. **Hauser H, et al.** 2010. HIV-1 Vpu and HIV-2 Env counteract BST-2/tetherin by sequestration in a perinuclear compartment. Retrovirology 7:51.
14. **Ito M, et al.** 2002. NOD/SCID/γ_c^{null} mouse: an excellent recipient mouse model for engraftment of human cells. Blood 100:3175–3182.
15. **Jia B, et al.** 2009. Species-specific activity of SIV Nef and HIV-1 Vpu in overcoming restriction by tetherin/BST2. PLoS Pathog. 5:e1000429.
16. **Jolly C, Booth NJ, Neil SJ.** 2010. Cell-cell spread of human immunodeficiency virus type 1 overcomes tetherin/BST-2-mediated restriction in T cells. J. Virol. 84:12185–12199.
17. **Jolly C, Mitar I, Sattentau QJ.** 2007. Adhesion molecule interactions facilitate human immunodeficiency virus type 1-induced virological synapse formation between T cells. J. Virol. 81:13916–13921.
18. **Jolly C, Mitar I, Sattentau QJ.** 2007. Requirement for an intact T-cell actin and tubulin cytoskeleton for efficient assembly and spread of human immunodeficiency virus type 1. J. Virol. 81:5547–5560.
19. **Jolly C, Sattentau QJ.** 2007. Human immunodeficiency virus type 1 assembly, budding, and cell-cell spread in T cells take place in tetraspanin-enriched plasma membrane domains. J. Virol. 81:7873–7884.
20. **Jolly C, Sattentau QJ.** 2005. Human immunodeficiency virus type 1 virological synapse formation in T cells requires lipid raft integrity. J. Virol. 79:12088–12094.
21. **Jolly C, Sattentau QJ.** 2007. Regulated secretion from CD4^{+} T cells. Trends Immunol. 28:474–481.
22. **Jolly C, Sattentau QJ.** 2004. Retroviral spread by induction of virological synapses. Traffic 5:643–650.
23. **Jouvenet N, et al.** 2009. Broad-spectrum inhibition of retroviral and filoviral particle release by tetherin. J. Virol. 83:1837–1844.
24. **Kaletsky RL, Francica JR, Agrawal-Gamse C, Bates P.** 2009. Tetherin-mediated restriction of filovirus budding is antagonized by the Ebola glycoprotein. Proc. Natl. Acad. Sci. U. S. A. 106:2886–2891.
25. **Kawano Y, et al.** 1997. Mutational analysis of human immunodeficiency virus type 1 (HIV-1) accessory genes: requirement of a site in the nef gene for HIV-1 replication in activated CD4^{+} T cells *in vitro* and *in vivo*. J. Virol. 71:8456–8466.
26. **Kirchhoff F.** 2010. Immune evasion and counteraction of restriction factors by HIV-1 and other primate lentiviruses. Cell Host Microbe 8:55–67.
27. **Kobayashi T, et al.** 2011. Identification of amino acids in the human tetherin transmembrane domain responsible for HIV-1 Vpu interaction and susceptibility. J. Virol. 85:932–945.
28. **Kuhl BD, et al.** 2010. Tetherin restricts direct cell-to-cell infection of HIV-1. Retrovirology 7:115.
29. **Lama J, Mangasarian A, Trono D.** 1999. Cell-surface expression of CD4 reduces HIV-1 infectivity by blocking Env incorporation in a Nef- and Vpu-inhibitable manner. Curr. Biol. 9:622–631.
30. **Le Tortorec A, Neil SJ.** 2009. Antagonism to and intracellular sequestration of human tetherin by the human immunodeficiency virus type 2 envelope glycoprotein. J. Virol. 83:11966–11978.
31. **Levesque K, Finzi A, Binette J, Cohen EA.** 2004. Role of CD4 receptor down-regulation during HIV-1 infection. Curr. HIV Res. 2:51–59.
32. **Levesque K, Zhao YS, Cohen EA.** 2003. Vpu exerts a positive effect on HIV-1 infectivity by down-modulating CD4 receptor molecules at the surface of HIV-1-producing cells. J. Biol. Chem. 278:28346–28353.
33. **Maldarelli F, Chen MY, Willey RL, Strebel K.** 1993. Human immunodeficiency virus type 1 Vpu protein is an oligomeric type I integral membrane protein. J. Virol. 67:5056–5061.
34. **Mansouri M, et al.** 2009. Molecular mechanism of BST2/tetherin down-regulation by K5/MIR2 of Kaposi's sarcoma-associated herpesvirus. J. Virol. 83:9672–9681.
35. **Margottin F, et al.** 1998. A novel human WD protein, h-beta TrCp, that interacts with HIV-1 Vpu connects CD4 to the ER degradation pathway through an F-box motif. Mol. Cell 1:565–574.
36. **Martin N, Sattentau Q.** 2009. Cell-to-cell HIV-1 spread and its implications for immune evasion. Curr. Opin. HIV AIDS 4:143–149.
37. **Mitchell RS, et al.** 2009. Vpu antagonizes BST-2-mediated restriction of HIV-1 release via β-TrCP and endo-lysosomal trafficking. PLoS Pathog. 5:e1000450.
38. **Miyagi E, Andrew AJ, Kao S, Strebel K.** 2009. Vpu enhances HIV-1 virus release in the absence of Bst-2 cell surface down-modulation and intracellular depletion. Proc. Natl. Acad. Sci. U. S. A. 106:2868–2873.
39. **Moyer CL, Wiethoff CM, Maier O, Smith JG, Nemerow GR.** 2011. Functional genetic and biophysical analyses of membrane disruption by human adenovirus. J. Virol. 85:2631–2641.
40. **Neil SJ, Eastman SW, Jouvenet N, Bieniasz PD.** 2006. HIV-1 Vpu promotes release and prevents endocytosis of nascent retrovirus particles from the plasma membrane. PLoS Pathog. 2:e39.
41. **Neil SJ, Sandrin V, Sundquist WI, Bieniasz PD.** 2007. An interferon-alpha-induced tethering mechanism inhibits HIV-1 and Ebola virus particle release but is counteracted by the HIV-1 Vpu protein. Cell Host Microbe 2:193–203.

42. **Neil SJ, Zang T, Bieniasz PD.** 2008. Tetherin inhibits retrovirus release and is antagonized by HIV-1 Vpu. Nature **451**:425–430.
43. **Ni H, Barrett AD.** 1998. Attenuation of Japanese encephalitis virus by selection of its mouse brain membrane receptor preparation escape variants. Virology **241**:30–36.
44. **Nie C, et al.** 2009. Selective infection of $CD4^+$ effector memory T lymphocytes leads to preferential depletion of memory T lymphocytes in R5 HIV-1-infected humanized NOD/SCID/IL-2Rγ^{null} mice. Virology **394**: 64–72.
45. **Okuma K, et al.** 2008. Interleukin-4-transgenic hu-PBL-SCID mice: a model for the screening of antiviral drugs and immunotherapeutic agents against X4 HIV-1 viruses. J. Infect. Dis. **197**:134–141.
46. **Pardieu C, et al.** 2010. The RING-CH ligase K5 antagonizes restriction of KSHV and HIV-1 particle release by mediating ubiquitin-dependent endosomal degradation of tetherin. PLoS Pathog. **6**:e1000843.
47. **Radoshitzky SR, et al.** 2010. Infectious Lassa virus, but not filoviruses, is restricted by BST-2/tetherin. J. Virol. **84**:10569–10580.
48. **Ross TM, Oran AE, Cullen BR.** 1999. Inhibition of HIV-1 progeny virion release by cell-surface CD4 is relieved by expression of the viral Nef protein. Curr. Biol. **9**:613–621.
49. **Sakuma T, Noda T, Urata S, Kawaoka Y, Yasuda J.** 2009. Inhibition of Lassa and Marburg virus production by tetherin. J. Virol. **83**:2382–2385.
50. **Sato H, Orenstein J, Dimitrov D, Martin M.** 1992. Cell-to-cell spread of HIV-1 occurs within minutes and may not involve the participation of virus particles. Virology **186**:712–724.
51. **Sato K, et al.** 2008. Modulation of human immunodeficiency virus type 1 infectivity through incorporation of tetraspanin proteins. J. Virol. **82**: 1021–1033.
52. **Sato K, et al.** 2010. Remarkable lethal G-to-A mutations in *vif*-proficient HIV-1 provirus by individual APOBEC3 proteins in humanized mice. J. Virol. **84**:9546–9556.
53. **Sato K, Koyanagi Y.** 2011. The mouse is out of the bag: insights and perspectives on HIV-1-infected humanized mouse models. Exp. Biol. Med. (Maywood) **236**:977–985.
54. **Sato K, et al.** 2011. A novel animal model of Epstein-Barr virus-associated hemophagocytic lymphohistiocytosis in humanized mice. Blood **117**: 5663–5673.
55. **Sato K, et al.** 2010. Dynamics of memory and naive $CD8^+$ T lymphocytes in humanized NOD/SCID/IL-2Rγ^{null} mice infected with CCR5-tropic HIV-1. Vaccine **28**(Suppl 2):B32–B37.
56. **Sato K, et al.** 2009. Comparative study on the effect of human BST-2/Tetherin on HIV-1 release in cells of various species. Retrovirology **6**:53.
57. **Sattentau Q.** 2008. Avoiding the void: cell-to-cell spread of human viruses. Nat. Rev. Microbiol. **6**:815–826.
58. **Sauter D, et al.** 2009. Tetherin-driven adaptation of Vpu and Nef function and the evolution of pandemic and nonpandemic HIV-1 strains. Cell Host Microbe **6**:409–421.
59. **Schindler M, et al.** 2010. Vpu serine 52 dependent counteraction of tetherin is required for HIV-1 replication in macrophages, but not in *ex vivo* human lymphoid tissue. Retrovirology **7**:1.
60. **Schubert U, et al.** 1998. CD4 glycoprotein degradation induced by human immunodeficiency virus type 1 Vpu protein requires the function of proteasomes and the ubiquitin-conjugating pathway. J. Virol. **72**:2280–2288.
61. **Schubert U, et al.** 1996. The two biological activities of human immunodeficiency virus type 1 Vpu protein involve two separable structural domains. J. Virol. **70**:809–819.
62. **Schubert U, Bour S, Willey RL, Strebel K.** 1999. Regulation of virus release by the macrophage-tropic human immunodeficiency virus type 1 AD8 isolate is redundant and can be controlled by either Vpu or Env. J. Virol. **73**:887–896.
63. **Schubert U, Clouse KA, Strebel K.** 1995. Augmentation of virus secretion by the human immunodeficiency virus type 1 Vpu protein is cell type independent and occurs in cultured human primary macrophages and lymphocytes. J. Virol. **69**:7699–7711.
64. **Shah AH, et al.** 2010. Degranulation of natural killer cells following interaction with HIV-1-infected cells is hindered by downmodulation of NTB-A by Vpu. Cell Host Microbe **8**:397–409.
65. **Strebel K, Klimkait T, Martin MA.** 1988. A novel gene of HIV-1, vpu, and its 16-kilodalton product. Science **241**:1221–1223.
66. **Theodore TS, et al.** 1996. Construction and characterization of a stable full-length macrophage-tropic HIV type 1 molecular clone that directs the production of high titers of progeny virions. AIDS Res. Hum. Retroviruses **12**:191–194.
67. **Van Damme N, et al.** 2008. The interferon-induced protein BST-2 restricts HIV-1 release and is downregulated from the cell surface by the viral Vpu protein. Cell Host Microbe **3**:245–252.
68. **Varthakavi V, Smith RM, Bour SP, Strebel K, Spearman P.** 2003. Viral protein U counteracts a human host cell restriction that inhibits HIV-1 particle production. Proc. Natl. Acad. Sci. U. S. A. **100**:15154–15159.
69. **Watanabe R, Leser GP, Lamb RA.** 2011. Influenza virus is not restricted by tetherin whereas influenza VLP production is restricted by tetherin. Virology **417**:50–56.
70. **Wei X, et al.** 2002. Emergence of resistant human immunodeficiency virus type 1 in patients receiving fusion inhibitor (T-20) monotherapy. Antimicrob. Agents Chemother. **46**:1896–1905.
71. **Weidner JM, et al.** 2010. Interferon-induced cell membrane proteins, IFITM3 and tetherin, inhibit vesicular stomatitis virus infection via distinct mechanisms. J. Virol. **84**:12646–12657.
72. **Willey RL, Maldarelli F, Martin MA, Strebel K.** 1992. Human immunodeficiency virus type 1 Vpu protein induces rapid degradation of CD4. J. Virol. **66**:7193–7200.
73. **Zhang F, et al.** 2009. Nef proteins from simian immunodeficiency viruses are tetherin antagonists. Cell Host Microbe **6**:54–67.

JVI
Journals.ASM.org

Association of Major Histocompatibility Complex Class I Haplotypes with Disease Progression after Simian Immunodeficiency Virus Challenge in Burmese Rhesus Macaques

Takushi Nomura,[a,b] Hiroyuki Yamamoto,[a] Teiichiro Shiino,[a] Naofumi Takahashi,[a,b] Taku Nakane,[a,b] Nami Iwamoto,[a,b] Hiroshi Ishii,[a,b] Tetsuo Tsukamoto,[b] Miki Kawada,[b] Saori Matsuoka,[a] Akiko Takeda,[a] Kazutaka Terahara,[c] Yasuko Tsunetsugu-Yokota,[c] Naoko Iwata-Yoshikawa,[d] Hideki Hasegawa,[d] Tetsutaro Sata,[d] Taeko K. Naruse,[e] Akinori Kimura,[e] and Tetsuro Matano[a,b]

AIDS Research Center, National Institute of Infectious Diseases, Toyama, Shinjuku-ku, Tokyo, Japan[a]; The Institute of Medical Science, The University of Tokyo, Shirokanedai, Minato-ku, Tokyo, Japan[b]; Department of Immunology, National Institute of Infectious Diseases, Toyama, Shinjuku-ku, Tokyo, Japan[c]; Department of Pathology, National Institute of Infectious Diseases, Toyama, Shinjuku-ku, Tokyo, Japan[d]; and Department of Molecular Pathogenesis, Medical Research Institute, Tokyo Medical and Dental University, Kandasurugadai, Chiyoda-ku, Tokyo, Japan[e]

Nonhuman primate AIDS models are essential for the analysis of AIDS pathogenesis and the evaluation of vaccine efficacy. Multiple studies on human immunodeficiency virus and simian immunodeficiency virus (SIV) infection have indicated the association of major histocompatibility complex class I (MHC-I) genotypes with rapid or slow AIDS progression. The accumulation of macaque groups that share not only a single MHC-I allele but also an MHC-I haplotype consisting of multiple polymorphic MHC-I loci would greatly contribute to the progress of AIDS research. Here, we investigated SIVmac239 infections in four groups of Burmese rhesus macaques sharing individual MHC-I haplotypes, referred to as A, E, B, and J. Out of 20 macaques belonging to A^+ ($n = 6$), E^+ ($n = 6$), B^+ ($n = 4$), and J^+ ($n = 4$) groups, 18 showed persistent viremia. Fifteen of them developed AIDS in 0.5 to 4 years, with the remaining three at 1 or 2 years under observation. A^+ animals, including two controllers, showed slower disease progression, whereas J^+ animals exhibited rapid progression. E^+ and B^+ animals showed intermediate plasma viral loads and survival periods. Gag-specific $CD8^+$ T-cell responses were efficiently induced in A^+ animals, while Nef-specific $CD8^+$ T-cell responses were in A^+, E^+, and B^+ animals. Multiple comparisons among these groups revealed significant differences in survival periods, peripheral $CD4^+$ T-cell decline, and SIV-specific $CD4^+$ T-cell polyfunctionality in the chronic phase. This study indicates the association of MHC-I haplotypes with AIDS progression and presents an AIDS model facilitating the analysis of virus-host immune interaction.

Virus-specific $CD8^+$ cytotoxic T lymphocytes (CTLs) are major effectors against persistent virus infections (13, 44). In virus-infected cells, viral antigen-derived peptides (epitopes) are bound to major histocompatibility complex class I (MHC-I) molecules and presented on the cell surface. Viral peptide-specific CTLs recognize the peptide-MHC-I complexes by their T-cell receptors. CTL effectors deliver cell death via apoptosis as well as lysis (15, 48).

Human immunodeficiency virus type 1 (HIV-1) infection induces persistent viral replication leading to AIDS progression. CTL responses play a central role in the suppression of HIV-1 replication (6, 18, 25, 32, 43). Multiple studies on HIV-1-infected individuals have shown an association of HLA genotypes with rapid or delayed AIDS progression (14, 23, 27, 51, 54). For instance, HIV-1-infected individuals possessing *HLA-B*57* tend to show a better prognosis with lower viral loads, implicating HLA-B*57-restricted epitope-specific CTL responses in this viral control (3, 33, 34). In contrast, the association of *HLA-B*35* with rapid disease progression has been indicated (8).

Nonhuman primate AIDS models are important for the analysis of AIDS pathogenesis and the evaluation of vaccine efficacy (5, 35, 47). Models of simian immunodeficiency virus (SIV) infection in macaques are widely used currently (12, 22). Indian rhesus macaques possessing certain MHC-I alleles, such as *Mamu-A*01*, *Mamu-B*08*, and *Mamu-B*17*, tend to show lower set point plasma viral loads in SIV infection (30, 36, 37, 59). Regarding MHC-I alleles, humans have a single polymorphic HLA-A, HLA-B, and HLA-C locus per chromosome, whereas MHC-I haplotypes in macaques have variable numbers of expressed polymorphic MHC-I loci (7, 9, 26, 41). Thus, the accumulation of multiple macaque groups, each sharing a different MHC-I haplotype, would contribute to the precise analysis of SIV infection.

We have been working on the establishment of an AIDS model using Burmese rhesus macaques sharing MHC-I haplotypes (38, 50). In the present study, we have focused on SIV infection in four groups of Burmese rhesus macaques, each consisting of four or more animals. These groups share MHC-I haplotypes *90-120-Ia* (referred to as A), *90-010-Ie* (E), *90-120-Ib* (B), and *90-088-Ij* (J), respectively. The analysis of SIVmac239 infection among these groups revealed differences in plasma viral loads, peripheral $CD4^+$ T cell counts, survival periods, virus-specific CTL responses, and T-cell polyfunctionality. Our results indicate the association of MHC-I haplotypes with disease progression in SIV infection and present a sophisticated model of SIV infection.

Received 11 December 2011 Accepted 27 March 2012
Published ahead of print 4 April 2012
Address correspondence to Tetsuro Matano, tmatano@nih.go.jp.

doi:10.1128/JVI.07077-11

TABLE 1 MHC-I haplotypes

MHC-I haplotype	Confirmed MHC-I allele(s)	
	Mamu-A	*Mamu-B*
A (*90-120-Ia*)	*A1*043:01, A1*065:01*	*B*061:03, B*068:04, B*089:01*
E (*90-010-Ie*)	*A1*066:01*	*B*005:02, B*015:04*
B (*90-120-Ib*)	*A1*018:08, A2*005:31*	*B*036:03, B*037:01, B*043:01, B*162:01*
J (*90-088-Ij*)	*A1*008:01*	*B*007:02, B*039:01*

MATERIALS AND METHODS

Animal experiments. We examined SIV infections in four groups of Burmese rhesus macaques having MHC-I haplotypes *90-120-Ia* (A) (n = 6), *90-010-Ie* (E) (n = 6), *90-120-Ib* (B) (n = 4), and *90-088-Ij* (J) (n = 4). Macaques R02-007, R06-037, R07-001, R07-004, R07-009, R01-011, R05-007, R06-038, R06-001, R02-004, R04-014, and R06-022, which were used as controls in previous experiments (49, 53, 58), were included in the present study. The determination of MHC-I haplotypes was based on the family study in combination with the reference strand-mediated conformation analysis (RSCA) of *Mamu-A* and *Mamu-B* genes as described previously (31). Briefly, locus-specific reverse transcription-PCR (RT-PCR) products from total cellular RNAs were prepared and used to form heteroduplex DNAs with a 5′ Cy5-labeled reference strand (50). The heteroduplex DNAs were subjected to a 6% nondenaturing acrylamide gel electrophoresis to identify the patterns of MHC-I haplotypes. In addition, although recombination events could not be ruled out, major *Mamu-A* and *Mamu-B* alleles were determined by cloning the RT-PCR products and sequencing at least 48 clones for each locus from each subject as described previously (38). Because we used locus-specific primers in the RT-PCR, which were designed on the basis of known alleles (31, 38), MHC class I alleles harboring mismatches with the primer sequences or alleles of low expression would not be amplified well, hence there was a limitation that not all of the MHC class I alleles could be detected in our study. Confirmed *Mamu-A* and *Mamu-B* alleles in MHC-I haplotypes A, E, B, and

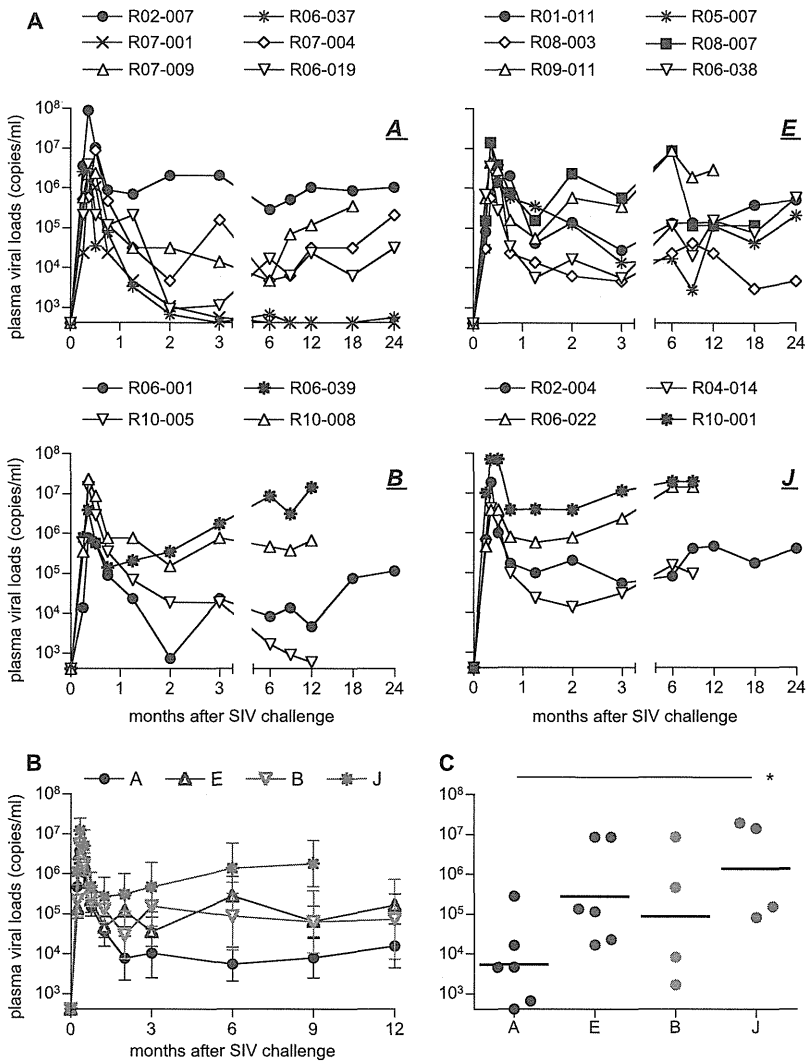

FIG 1 Plasma viral loads after SIVmac239 challenge. Plasma viral loads (SIV *gag* RNA copies/ml plasma) were determined as described previously (31). The lower limit of detection is approximately 4×10^2 copies/ml. (A) Changes in plasma viral loads after challenge in A^+ (upper left), E^+ (upper right), B^+ (lower left), and J^+ (lower right) macaques. (B) Changes in geometric means of plasma viral loads after challenge in A^+ (black), E^+ (blue), B^+ (green), and J^+ (red) animals. (C) Comparison of plasma viral loads at 6 months among four groups. Those of A^+ animals were significantly lower than those of J^+ animals (P = 0.0444 by one-way ANOVA and Tukey-Kramer's multiple-comparison test).

J are shown in Table 1 (38). All animals were unvaccinated and challenged intravenously with 1,000 $TCID_{50}$ (50% tissue culture infective doses) of SIVmac239 (22). At 1 week after challenge, macaques R06-019, R06-038, and R10-008 were intravenously infused with 300 mg of nonspecific immunoglobulin G purified from uninfected rhesus macaques (57). Fifteen animals were euthanized when they showed typical signs of AIDS, such as reduction in peripheral $CD4^+$ T-cell counts, loss of body weight, diarrhea, and general weakness. Autopsy revealed lymphoatrophy or postpersistent generalized lymphadenopathy conditions consistent with AIDS (20). All animals were maintained in accordance with the guidelines for animal experiments at the National Institute of Biomedical Innovation and National Institute of Infectious Diseases.

Analysis of SIV antigen-specific $CD8^+$ T-cell responses. SIV antigen-specific $CD8^+$ T-cell responses were measured by the flow-cytometric analysis of gamma interferon (IFN-γ) induction as described previously (17). Peripheral blood mononuclear cells (PBMCs) were cocultured with autologous herpesvirus papioimmortalized B-lymphoblastoid cell lines (B-LCLs) pulsed with peptide pools using panels of overlapping peptides spanning the entire SIVmac239 Gag, Pol, Vif, Vpx, Vpr, Tat, Rev, Env, and Nef amino acid sequences. Intracellular IFN-γ staining was performed using a Cytofix Cytoperm kit (BD, Tokyo, Japan). Fluorescein isothiocyanate-conjugated anti-human CD4 (BD), peridinin chlorophyll protein (PerCP)-conjugated anti-human CD8 (BD), allophycocyanin Cy7 (APC-Cy7)-conjugated anti-human CD3 (BD), and phycoerythrin (PE)-conjugated anti-human IFN-γ antibodies (Biolegend, San Diego, CA) were used. Specific T-cell levels were calculated by subtracting nonspecific IFN-γ^+ T-cell frequencies from those after peptide-specific stimulation. Specific T-cell levels of less than 100 cells per million PBMCs were considered negative. Using PBMCs obtained from four SIV-infected macaques, we compared antigen-specific $CD8^+$ T-cell frequencies measured by this method (using peptide-pulsed B-LCLs) to those measured by the flow-cytometric analysis of IFN-γ induction after a pulse of PBMCs with peptides (without using B-LCLs). The levels of the former tended to be slightly higher than those of the latter. Specific $CD8^+$ T-cell responses, which were shown to be 100 to 200 cells per million PBMCs by the former method using B-LCLs, were undetectable by the latter method.

Sequencing analysis of plasma viral genomes. Viral RNAs were extracted using the High Pure Viral RNA kit (Roche Diagnostics, Tokyo, Japan) from macaque plasma obtained around 1 year after challenge. Fragments of cDNAs encoding SIVmac239 Gag, Pol, Vif, Vpx, Vpr, Tat, Rev, and Nef were amplified by nested RT-PCR from plasma RNAs and subjected to direct sequencing by using dye terminator chemistry and an automated DNA sequencer (Applied Biosystems, Tokyo, Japan) as described before (19). Predominant nonsynonymous mutations were determined. The Env-coding region, which is known to have multiple antibody-related mutations, was not included for the analysis.

Analysis of SIV-specific polyfunctional T-cell responses. To analyze polyfunctionality in SIV-specific T-cell responses, we examined the SIV-specific induction of IFN-γ, tumor necrosis factor alpha (TNF-α), interleukin-2 (IL-2), macrophage inflammatory protein 1β (MIP-1β), and CD107a in $CD4^+$ and $CD8^+$ T cells as described previously (58), with some modifications. Around 8 months after challenge, PBMCs were cocultured with B-LCLs infected with vesicular stomatitis virus G protein-pseudotyped SIVGP1 for the SIV-specific stimulation or mock-infected B-LCLs for nonspecific stimulation. The pseudotyped virus was obtained by the cotransfection of 293T cells with a vesicular stomatitis virus G protein expression plasmid and an *env* and *nef* deletion-containing simian-human immunodeficiency virus molecular clone (SIVGP1) DNA that has the genes encoding SIVmac239 Gag, Pol, Vif, Vpx, and a part of Vpr (31, 46). Immunostaining was performed using a Fix & Perm fixation and permeabilization kit (Invitrogen, Tokyo, Japan) and the following monoclonal antibodies: APC-Cy7-conjugated anti-human CD3 (BD), PE-Texas red-conjugated anti-human CD4 (Invitrogen), Alexa Fluor 700-conjugated anti-human CD8 (BD), PE-Cy7-conjugated anti-human IFN-γ (eBioscience, San Diego, CA), Pacific blue-conjugated anti-human TNF-α (Biolegend), PerCP-Cy5.5-conjugated anti-human IL-2 (Biolegend), PE-conjugated anti-human MIP-1β (BD), and Alexa Fluor 647-conjugated anti-human CD107a (Biolegend). Dead cells were stained using Live/Dead Fixable Dead Cell Stain kit (Invitrogen). Analysis was carried out using PESTLE (version 1.6.1) and SPICE (version 5.2) programs as described previously (42). The polyfunctionality (polyfunctional value) was shown as mean numbers of induced factors among the five (IFN-γ, TNF-α, IL-2, MIP-1β, and CD107a) per SIV-specific T cell.

Statistical analysis. Statistical analyses were performed using R software (R Development Core Team). Comparisons were performed by one-way analysis of variance (ANOVA) and Tukey-Kramer's multiple comparison test with significance levels set at $P < 0.05$. Correlation was analyzed by the Pearson test.

TABLE 2 List of macaques in this study

MHC-I haplotype	Macaque	Disease progression	Euthanasia time point (mo)
A	R02-007	AIDS	42
A	R06-037	No	49
A	R07-001	No	49
A	R07-004	AIDS	40
A	R07-009	AIDS	17
A	R06-019	AIDS	43
E	R01-011	AIDS	24
E	R05-007	AIDS	37
E	R08-003	Under observation (24 months)	
E	R08-007	AIDS	20
E	R09-011	AIDS	12
E	R06-038	AIDS	22
B	R06-001	AIDS	34
B	R06-039	AIDS	13
B	R10-005	Under observation (12 months)	
B	R10-008	Under observation (12 months)	
J	R02-004	AIDS	37
J	R04-014	AIDS	9
J	R06-022	AIDS	5
J	R10-001	AIDS	9

RESULTS

SIV infection in Burmese rhesus macaques. We accumulated four groups of unvaccinated, SIVmac239-infected Burmese rhesus macaques, groups A^+ ($n = 6$), E^+ ($n = 6$), B^+ ($n = 4$), and J^+ ($n = 4$), sharing MHC-I haplotypes A (*90-120-Ia*), E (*90-010-Ie*), B (*90-120-Ib*), and J (*90-088-Ij*), respectively, to compare SIV infections among these groups (Table 1). Out of these 20 animals, 18 showed persistent viremia (geometric mean plasma viral loads at 6 months of 1.6×10^5 copies/ml), while in the remaining two (A^+ macaques R06-037 and R07-001), plasma viral loads became less than 10^3 copies/ml or were undetectable at the set point (Fig. 1A). The former 18 animals are referred to as noncontrollers and the latter two as controllers in this study. Fifteen noncontrollers were euthanized with AIDS progression in 4 years (geometric mean survival period of 24 months), and the remaining three, after 1 or 2 years, are under observation (Table 2).

Group A^+ macaques, including two controllers, showed lower set point viral loads, whereas group J^+ macaques had higher viral loads (Fig. 1B). Viral loads in group E^+ and B^+ macaques were at intermediate levels. Multiple comparisons indicated significant

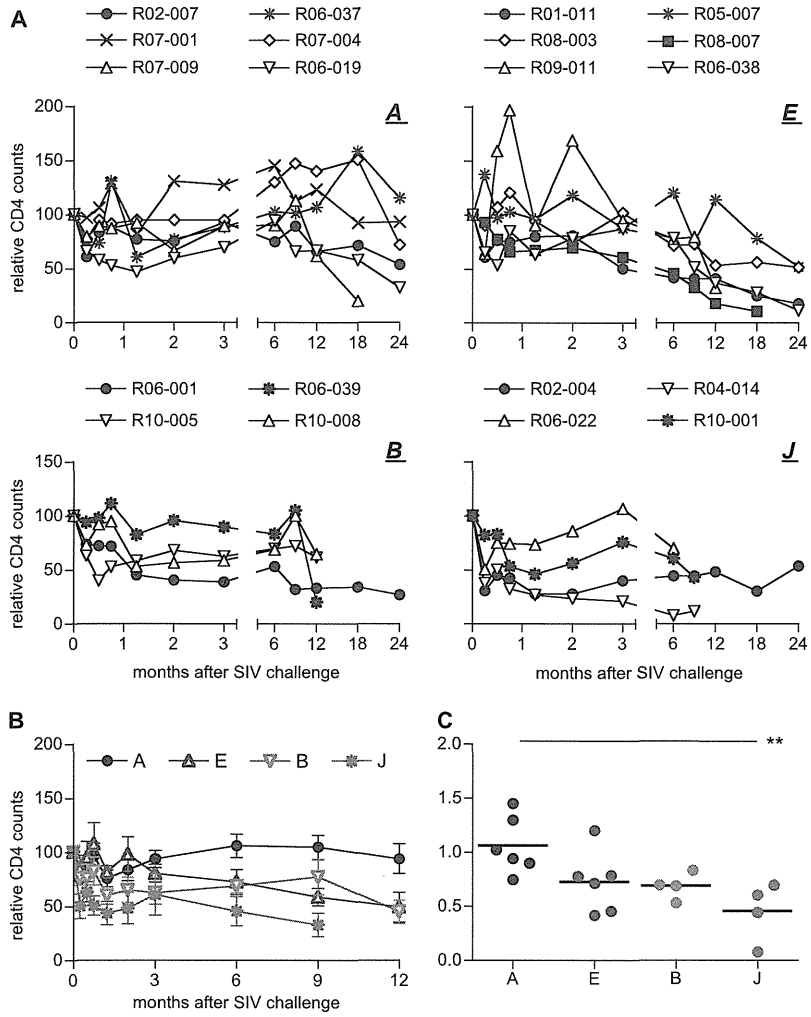

FIG 2 Relative $CD4^+$ T-cell counts after SIVmac239 challenge. (A) Relative $CD4^+$ T-cell counts after challenge in A^+ (upper left), E^+ (upper right), B^+ (lower left), and J^+ (lower right) macaques. For each animal, the peripheral CD4 counts relative to that at challenge (set at 100) are shown. (B) Changes in means of relative $CD4^+$ T-cell counts after challenge in A^+ (black), E^+ (blue), B^+ (green), and J^+ (red) animals. (C) Comparison of relative $CD4^+$ T-cell counts at 6 months among four groups. Those in J^+ animals were significantly lower than those in A^+ ($P = 0.0090$ by one-way ANOVA and Tukey-Kramer's multiple-comparison test).

differences in set point plasma viral loads between groups A^+ and J^+ (Fig. 1C).

Most noncontrollers showed a decline in peripheral $CD4^+$ T-cell counts (Fig. 2A). Relative $CD4^+$ T-cell counts in the chronic phase were the highest in group A^+ animals and the lowest in group J^+ animals. Multiple-comparison tests revealed significant differences in relative $CD4^+$ T-cell counts at 6 months between groups A^+ and J^+ (Fig. 2B and C). Furthermore, multiple comparisons among groups A^+, E^+, and J^+ found significant differences in survival periods, which were the longest in A^+ and the shortest in J^+ animals (Table 2 and Fig. 3). These results indicate an association of MHC-I haplotypes with AIDS progression after SIV challenge in Burmese rhesus macaques.

SIV antigen-specific $CD8^+$ T-cell responses. We analyzed SIV-specific $CD8^+$ T-cell responses at 3 months and 1 year after SIV challenge by the detection of antigen-specific IFN-γ induction to examine which antigen-specific $CD8^+$ T-cell responses were induced predominantly (Table 3). Analysis revealed the predominant induction of Gag-specific and Nef-specific $CD8^+$ T-cell responses in group A^+ animals and Nef-specific $CD8^+$ T-cell responses in groups E^+ and B^+. Vif-specific $CD8^+$ T-cell responses were detected in three J^+ animals but not macaque R06-022, which rapidly developed AIDS in 5 months without detectable SIV-specific $CD8^+$ T-cell responses.

There was no significant difference in whole SIV antigen-specific $CD8^+$ T-cell responses among these four groups, although those responses were marginal or undetectable in two of four J^+ animals (Fig. 4A). However, Gag-specific $CD8^+$ T-cell frequencies at 3 months were significantly higher in A^+ animals (Fig. 4B). The analysis of four groups revealed inverse correlations between Gag-specific $CD8^+$ T-cell frequencies and plasma viral loads at 3 months ($P = 0.0087$; $r^2 = 0.3407$; data not shown). Three groups of A^+, E^+, and B^+ animals tended to show higher Nef-specific $CD8^+$ T-cell responses than J^+ animals (Fig. 4C).

Viral genome mutations. We then analyzed mutations in viral cDNAs amplified from plasma RNAs of group A^+, E^+, and B^+

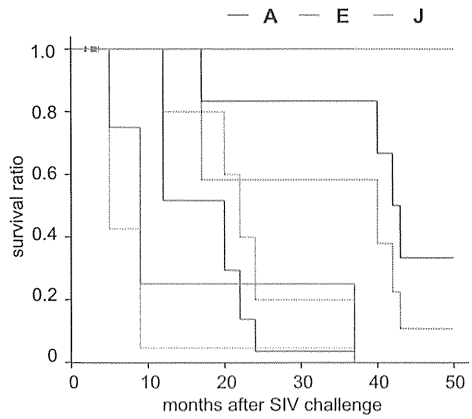

FIG 3 Kaplan-Meyer survival curves after SIVmac239 challenge in A^+, E^+, and J^+ macaques. Macaque R08-003, which is under observation, is not included. B^+ animals were excluded from this analysis because data on only two animals were available. We determined the Kaplan-Meyer estimate of the survival function of each group and then compared the three curves using the log-rank test (Mantel-Cox test). Analysis showed significant differences in survival curves (chi square, 9.9; $P = 0.007$ by log-rank test of Kaplan-Meyer estimates).

macaques around 1 year after SIV challenge. Nonsynonymous mutations detected predominantly were as shown in Fig. 5. Multiple comparisons among groups A^+, E^+, and B^+ (Fig. 6) showed no differences in total numbers of nonsynonymous mutations but revealed significantly higher numbers of *gag* mutations in A^+ animals. E^+ animals had higher numbers of *tat* mutations than A^+ animals. There was no significant difference in the numbers of mutations in other regions, including *nef*, among these groups. Group J^+ animals were not included in the multiple comparisons, because three of them were euthanized by 9 months. These three had lower numbers of nonsynonymous mutations before their death, possibly reflecting lower immune pressure.

Polyfunctionality in SIV-specific T-cell responses. Finally, we investigated T-cell polyfunctionality to compare T-cell functions (2, 4, 45) in these four groups having different viral loads. We analyzed the polyfunctionality of SIV-specific $CD4^+$ and $CD8^+$ T cells around 8 months after challenge by the detection of SIV-specific induction of IFN-γ, TNF-α, IL-2, MIP-1β, and CD107a. SIV-specific $CD4^+$ T-cell polyfunctionality inversely correlated with plasma viral loads at around 9 months (Fig. 7A). We also found an inverse correlation between SIV-specific $CD8^+$ T-cell polyfunctionality and viral loads (Fig. 7A). However, there was no

TABLE 3 SIV antigen-specific $CD8^+$ T-cell responses[a]

MHC-I haplotype and time point after challenge	Macaque	$CD8^+$ T-cell response to:								
		Gag	Pol	Vif	Vpx	Vpr	Tat	Rev	Env	Nef
3 mo										
A	R02-007	ND	ND	ND	ND	ND	ND	ND	ND	ND
A	R06-037	657	—	104	—	—	—	—	—	520
A	R07-001	193	—	—	—	—	—	—	—	322
A	R07-004	316	—	137	—	—	—	—	—	353
A	R07-009	440	—	124	—	—	—	—	100	247
A	R06-019	322	—	—	—	—	—	—	—	253
E	R01-011	—	—	186	—	—	—	—	—	—
E	R05-007	—	—	—	—	—	203	—	—	330
E	R08-003	—	—	—	—	—	—	—	—	213
E	R08-007	—	—	—	—	—	—	—	335	—
E	R09-011	—	—	807	—	307	—	—	1,598	2,327
E	R06-038	199	—	248	—	—	249	—	234	634
B	R06-001	—	107	253	172	—	—	—	114	313
B	R06-039	—	—	—	—	—	—	—	110	195
B	R10-005	163	172	—	1,033	141	—	579	—	1,554
B	R10-008	—	—	—	133	—	—	165	—	—
J	R02-004	—	—	171	—	—	145	—	382	117
J	R04-014	—	534	625	280	440	290	1,060	—	296
J	R06-022	—	—	—	—	—	—	—	—	—
J	R10-001	—	—	102	—	—	—	—	—	—
1 yr										
A	R02-007	—	—	119	—	—	—	—	112	250
A	R06-037	515	—	124	272	178	—	—	—	906
A	R07-001	126	—	—	—	—	—	—	—	180
A	R07-004	—	—	—	—	—	—	—	—	150
A	R07-009	254	120	173	—	112	—	—	215	166
A	R06-019	444	155	284	—	188	—	—	174	583
E	R01-011	160	—	—	—	—	—	—	—	228
E	R05-007	—	—	—	—	—	—	—	—	—
E	R08-003	—	—	—	—	—	—	—	—	537
E	R08-007	—	—	—	—	—	—	—	—	199
E	R09-011	—	159	—	—	—	—	150	259	102
E	R06-038	298	174	611	—	—	406	387	1,052	1,982
B	R06-001	—	—	—	—	—	—	—	127	140
B	R06-039	—	—	—	—	—	151	—	—	—
B	R10-005	185	—	—	—	—	—	—	—	—
B	R10-008	109	232	—	—	—	—	325	—	296
J	R02-004	158	—	—	—	—	—	—	—	—
J	R04-014[b]	114	141	178	—	—	360	288	—	142
J	R10-001[b]	—	—	—	—	—	—	—	—	—

[a] Responses were measured by the detection of antigen-specific IFN-γ induction. Macaque R06-022, euthanized at 5 months, is not included in the lower portion. Antigen-specific $CD8^+$ T-cell frequencies (per 1 million PBMCs) are shown. ND, not determined; —, undetectable (<100).

[b] At 9 months (before euthanasia).

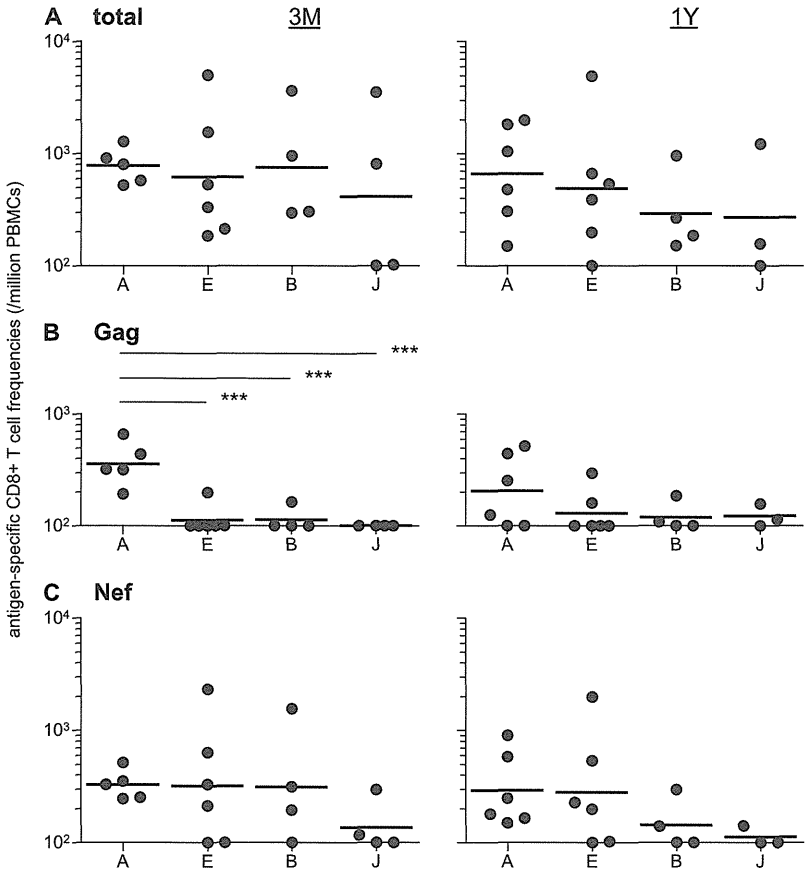

FIG 4 Comparison of SIV antigen-specific $CD8^+$ T-cell responses. Responses were measured by the detection of antigen-specific IFN-γ induction using PBMCs at 3 months (3 M; left) and at 1 year (1Y; right). (A) Whole SIV antigen-specific $CD8^+$ T-cell frequencies. The sum of Gag-, Pol-, Vif-, Vpx-, Vpr-, Tat-, Rev-, Env-, and Nef-specific $CD8^+$ T-cell frequencies in each animal is shown. (B) Gag-specific $CD8^+$ T-cell frequencies. The frequencies at 3 months in A^+ animals were significantly higher (A^+ and E^+, $P < 0.0001$; A^+ and B^+, $P = 0.0003$; A^+ and J^+, $P < 0.0001$ by one-way ANOVA and Tukey-Kramer's multiple-comparison test). (C) Nef-specific $CD8^+$ T-cell frequencies.

correlation between viral loads and total SIV-specific $CD4^+$ T-cell or $CD8^+$ T-cell frequencies (Fig. 7B). Polyfunctional T-cell responses tended to be higher in group A^+ and lower in group J^+. Multiple comparisons revealed significant differences in SIV-specific $CD4^+$ T-cell polyfunctionality with the highest in group A^+ and the lowest in group J^+ (Fig. 7C). These results may reflect difference in disease progression among these animals.

DISCUSSION

This study describes SIVmac239 infection in 20 Burmese rhesus macaques. Geometric means of set point plasma viral loads were approximately 10^5 copies/ml. The levels are considered lower than those usually observed in the widely used SIVmac239 infection model of Indian rhesus macaques (28, 55) but are higher than those typically observed in untreated humans infected with HIV-1. While two A^+ animals controlled SIV replication, the remaining 18 Burmese rhesus macaques failed to control viremia. Indeed, all of the animals in the three groups E^+, B^+, and J^+ showed persistent viremia. Those noncontrollers, including four A^+ animals, developed AIDS in 0.5 to 4 years. These results indicate that the SIVmac239 infection of Burmese rhesus macaques does serve as an AIDS model.

In the present study, we compared SIVmac239 infections among four groups sharing MHC-I haplotypes A, E, B, and J, respectively. These animals showed differences in plasma viral loads, peripheral $CD4^+$ T-cell counts, survival periods, patterns of viral antigen-specific $CD8^+$ T-cell responses, polyfunctionality of SIV-specific T-cell responses, and numbers of viral genome mutations. These results indicate the association of MHC-I haplotypes with AIDS progression. There has been a number of reports describing SIV infections in macaques sharing a single or a couple of MHC-I alleles, but few studies have examined SIV infection in macaques sharing an MHC-I haplotype (10, 11, 40). SIV infection induces multiple epitope-specific $CD8^+$ T-cell responses, and $CD8^+$ T-cell responses specific for some MHC-I-restricted epitopes can be affected by those specific for other MHC-I-restricted epitopes due to CTL immunodominance (16, 29, 52). Thus, the preparation of macaque groups sharing MHC-I genotypes at the haplotype level, as described in the present study, would contribute to the precise analysis of SIV infection. The establishment of groups sharing both MHC-I haplotypes (56) may be ideal, but the accumulation of macaque groups sharing even one MHC-I haplotype could lead to the constitution of a more sophisticated primate AIDS model.

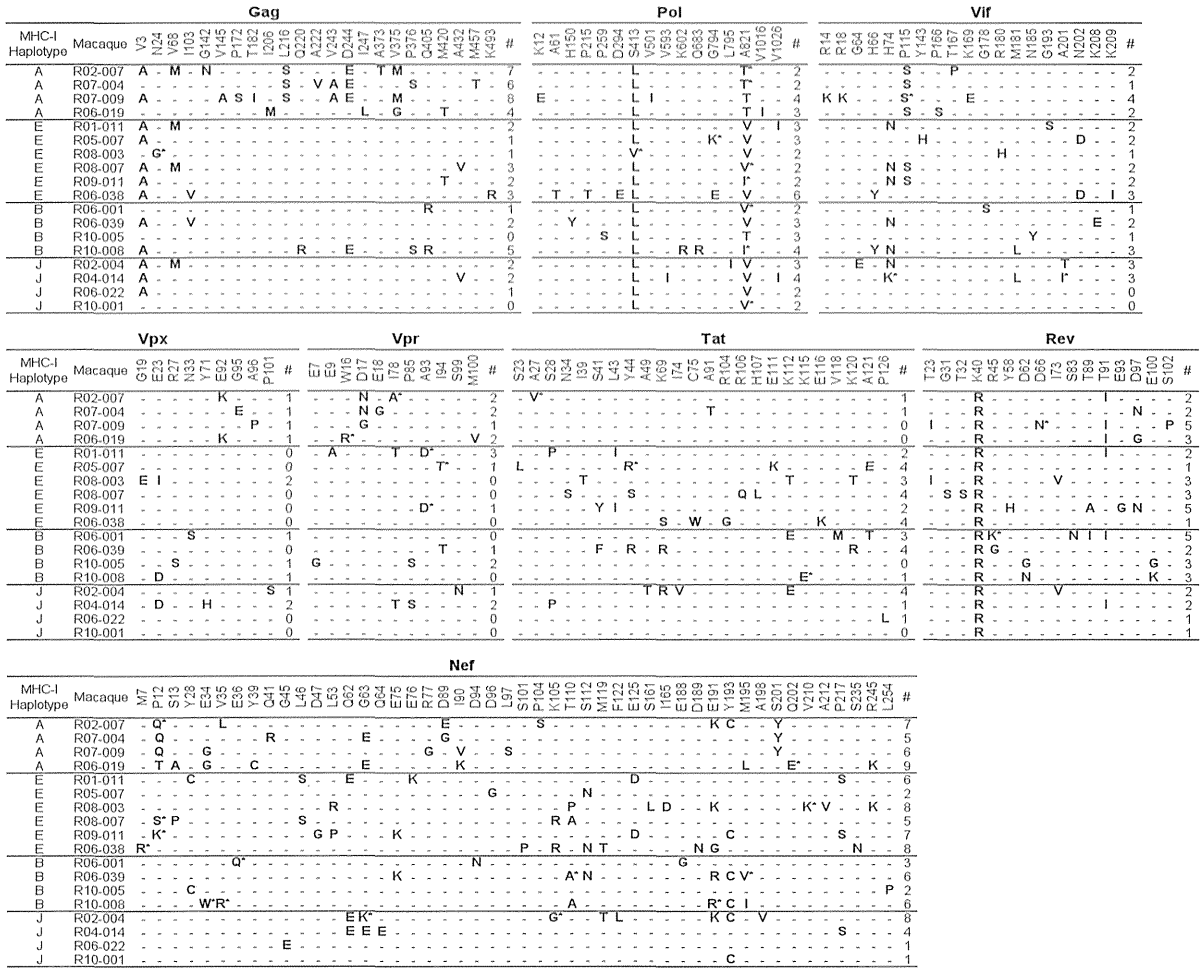

FIG 5 Predominant nonsynonymous mutations in viral cDNAs around 1 year after SIVmac239 challenge. Amino acid substitutions in SIV Gag, Pol, Vif, Vpx, Vpr, Tat, Rev, and Nef are shown. In three animals, R04-014, R06-022, and R10-001 in group J^+, data on the samples obtained before their death at 5 or 9 months after challenge are shown. Asterisks indicate the residues where different mutations were detected. It is known that amino acid substitutions at the Pol residues 413 and 821 and the Rev residue 40 are frequently observed in SIVmac239 infection and contribute to higher viral fitness *in vivo* (1, 39).

Various MHC-I alleles that do not consist of the first MHC-I haplotypes (A in A^+, E in E^+, B in B^+, and J in J^+ animals) were detected as shown in Table 4. Two A^+ macaques, R02-007 and R07-004, had two major alleles, *Mamu-A1*008:01* and *Mamu-B*007:02*, of MHC-I haplotype J, although their second MHC-I haplotype was not determined as J on the basis of information on the family tree. Even when these two animals were excluded from the A^+ group, multiple-comparison analyses showed significant

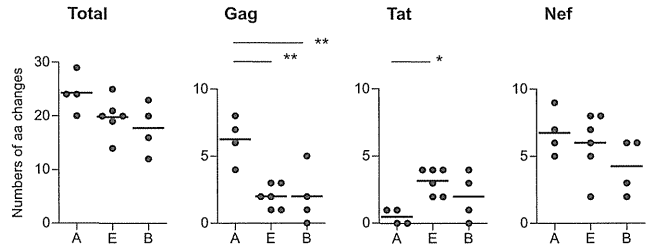

FIG 6 Comparison of the numbers of predominant nonsynonymous mutations in viral cDNAs around 1 year after SIVmac239 challenge among A^+, E^+, and B^+ macaques. J^+ animals were excluded from this analysis because three of them were euthanized by 1 year. The first graph (total) shows the sum of the numbers of amino acid substitutions in SIV Gag, Pol, Vif, Vpx, Vpr, Tat, Rev, and Nef. Gag, Tat, and Nef graphs show the numbers of Gag, Tat, and Nef amino acid substitutions, respectively. The numbers of Gag amino acid substitutions in A^+ animals were significantly higher than those in E^+ and B^+ animals (A^+ and E^+, $P = 0.0037$; A^+ and B^+, $P = 0.0069$ by one-way ANOVA and Tukey-Kramer's multiple-comparison test). The numbers of Tat amino acid substitutions in E^+ animals were significantly higher than those in A^+ animals ($P = 0.0140$).

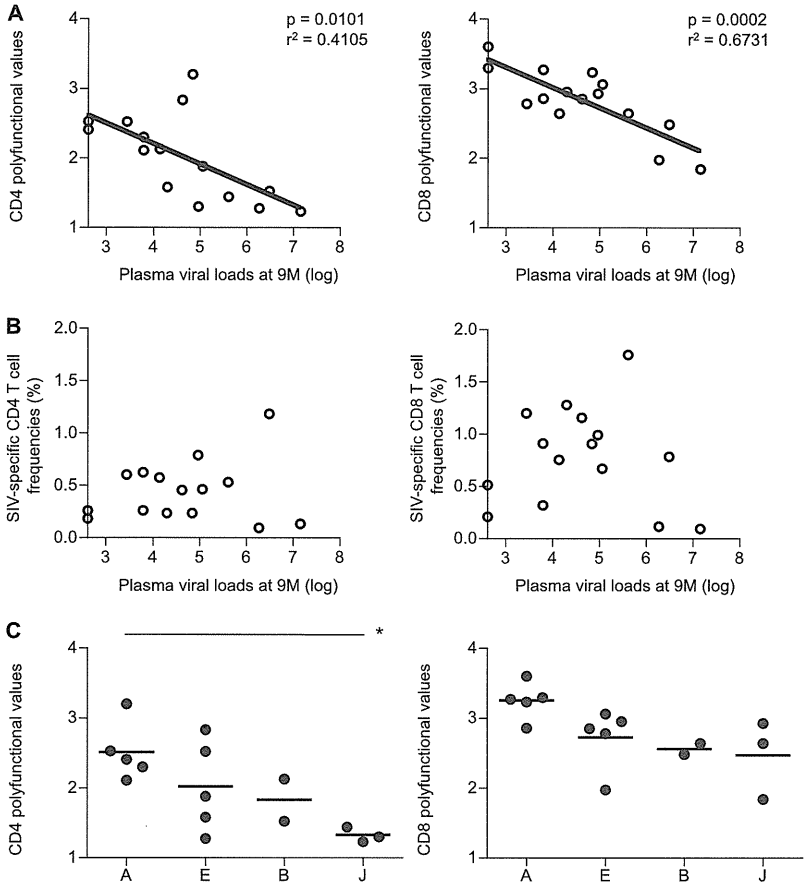

FIG 7 Polyfunctionality in SIV-specific $CD4^+$ and $CD8^+$ T cells around 8 months after SIVmac239 challenge. Samples of macaques R02-007 (A^+), R01-011 (E^+), R10-005 (B^+), R10-008 (B^+), and R10-001 (J^+) were unavailable. (A) Correlation analysis of plasma viral loads at 9 months with polyfunctionality (polyfunctional values) of SIV-specific $CD4^+$ (left) and $CD8^+$ (right) T cells. Viral loads inversely correlated with SIV-specific $CD4^+$ ($P = 0.0101$; $r^2 = 0.4105$) and $CD8^+$ ($P = 0.0002$; $r^2 = 0.6731$) T-cell polyfunctionality. (B) Correlation analysis of plasma viral loads at 9 months with SIV-specific $CD4^+$ (left) and $CD8^+$ (right) T-cell frequencies (frequencies of $CD4^+$ and $CD8^+$ T cells showing the SIV-specific induction of induction of IFN-γ, TNF-α, IL-2, MIP-1β, or CD107a). (C) SIV-specific $CD4^+$ (left) and $CD8^+$ (right) T-cell polyfunctionality in A^+ ($n = 5$), E^+ ($n = 5$), B^+ ($n = 2$), and J^+ ($n = 3$) macaques. Multiple comparisons among A^+, E^+, and J^+ animals (excluding the B^+ group with available data on only two animals) revealed significant difference in SIV-specific $CD4^+$ T-cell polyfunctionality (A^+ and J^+, $P = 0.0195$ by one-way ANOVA and Tukey-Kramer's multiple-comparison test).

differences in plasma viral loads, peripheral $CD4^+$ T-cell counts, survival periods, Gag-specific $CD8^+$ T-cell responses, and numbers of viral gag mutations. These two A^+ animals were noncontrollers, supporting the notion that CTL responses specific for Mamu-A1*008:01- or Mamu-B*007:02-restricted epitopes are not efficient or effective. In addition, several MHC-I alleles were shared in two or three animals, but the influence of these alleles on disease progression remains unclear.

In the group A^+ animals that showed lower viral loads and slower disease progression, Gag-specific $CD8^+$ T-cell responses were efficiently induced, and their frequencies were significantly higher than those in the other three groups. Furthermore, these A^+ animals had higher numbers of nonsynonymous *gag* mutations, possibly reflecting strong selective pressure by Gag-specific $CD8^+$ T-cell responses. Previously, $CD8^+$ T-cell responses specific for the $Gag_{206\text{-}216}$ (IINEEAADWDL) epitope restricted by MHC-I haplotype A-derived Mamu-A1*043:01 and the $Gag_{241\text{-}249}$ (SSVDEQIQW) epitope restricted by A-derived Mamu-A1*065:01 have been shown to exert strong suppressive pressure on SIV replication (19, 21). In the present study, most A^+ animals selected escape mutations from these $CD8^+$ T-cell responses, GagL216S (a mutation leading to a leucine [L]-to-serine [S] substitution at the 216th amino acid in Gag) and GagD244E (aspartic acid [D]-to-glutamic acid [E] substitution at the 244th amino acid) or I247L (isoleucine [I]-to-L substitution at the 247th amino acid). These results are consistent with recent findings suggesting the potential of Gag-specific $CD8^+$ T-cell responses to efficiently suppress HIV-1/SIV replication (24).

In SIV-infected A^+ animals, predominantly Nef-specific as well as Gag-specific $CD8^+$ T-cell responses were elicited. At 3 months postchallenge, all of the A^+ animals showed relatively similar levels of total antigen-specific, Gag-specific, and Nef-specific $CD8^+$ T-cell responses, and their deviations appeared to be less than those in the other three groups. This may reflect the diminished influence of the second MHC-I haplotypes in these A^+ animals in the early phase of SIV infection, i.e., $CD8^+$ T-cell responses specific for epitopes restricted by MHC-I molecules derived from the second haplotypes may be suppressed by dominant $CD8^+$ T-cell responses specific for A-derived MHC-I-restricted epitopes.

TABLE 4 Alleles in the second MHC-I haplotypes in macaques[a]

Group	Macaque	Allele(s)
A^+	R02-007	*A1*008:01, B*007:02*
A^+	R06-037	*A1*052:01, A2*005:13, B*089:02/03*[b]
A^+	R07-001	*A1*032:02, B*066:01*
A^+	R07-004	*A1*008:01, B*007:02, B*039:01*
A^+	R07-009	ND[c]
A^+	R06-019	*A1*032:02, A2*005:02, B*106:01, B*124:01*
E^+	R01-011	*A1*004:01, B*004:01, B*060:03, B*102:01*
E^+	R05-007	*A1*032:03, B*042:01, B*066:01, B*089:01*
E^+	R08-003	*B*074:02, B*101:01*
E^+	R08-007	*A2*005:10, B*054:02, B*061:04, B*063:02, B*124:01*
E^+	R09-011	*A1*041:02, B*061:02, B*068:04/05*[d]
E^+	R06-038	*A1*004:01, A-new,*[e] *B*001:01, B*007:02/03, B*017:03*
B^+	R06-001	*A1*008:01*
B^+	R06-039	*A1*032:02, B*004:01, B*033:01, B*066:01, B*102:01*
B^+	R10-005	*A1*003:01, B*019:01*
B^+	R10-008	*B*026:02, B*045:07, B*051:06*
J^+	R02-004	ND[f]
J^+	R04-014	*A4*014:03, B*071:01*
J^+	R06-022	*A5*030:06, B*102:01*
J^+	R10-001	*A1*004:01, B*026:02, B*043:01, B*073:01*

[a] Detected alleles not included in the first MHC-I haplotypes (A in A^+, E in E^+, B in B^+, or J in J^+ animals) are shown.
[b] The *Mamu-B* allele has sequences identical to *B*089:02* and *B*089:03* in exons 2 and 3.
[c] MHC-I alleles other than those consisting of the MHC-I haplotype A were not detected.
[d] The *Mamu-B* allele has sequences identical to *B*068:04* and *B*068:05* in exons 2 and 3.
[e] New *Mamu-A* allele 96% similar to *A1*018:03* by sequence homology in exons 2 and 3.
[f] MHC-I alleles other than those consisting of the MHC-I haplotype J were not detected.

Nef-specific $CD8^+$ T-cell responses were induced efficiently at 3 months or 1 year postchallenge in groups A^+, E^+, and B^+ but not in most J^+ animals, which showed higher viral loads and rapid disease progression. The former three groups had relatively higher numbers of nonsynonymous *nef* mutations, which correlated with Nef-specific $CD8^+$ T-cell responses at 1 year ($P = 0.0063$; $r^2 = 0.4765$; data not shown). Thus, these Nef-specific $CD8^+$ T-cell responses, whose suppressive pressure might be less than that of Gag-specific ones, may play roles in the suppression of SIV replication, while we have not determined Nef epitopes for those $CD8^+$ T-cell responses exerting strong suppressive pressure. No nef mutations common to each group were detected, which suggests multiple Nef epitope-specific $CD8^+$ T-cell responses. Regarding the Nef-specific $CD8^+$ T-cell responses in SIV-infected E^+ animals, some Nef epitopes are speculated to be restricted by E-derived MHC-I molecules. Our results, however, indicate that primary SIV infection induces no predominant $CD8^+$ T-cell responses specific for Gag epitopes restricted by E-derived MHC-I molecules in the early phase. In J^+ animals, we found no predominant $CD8^+$ T-cell responses specific for J-derived, MHC-I-restricted epitopes in the early phase of SIV infection.

This study indicates differences in the patterns of CTL immunodominance among these groups. Gag-specific $CD8^+$ T-cell responses were induced in group A^+, showing slower disease progression, and Nef-specific CTL responses were induced in those animals other than group J^+ animals, which showed rapid disease progression. These results can be reasonably explained by the differences in MHC-I haplotypes, although it is difficult to completely rule out the possibility of disease progression associating with other genes located around the MHC-I locus. In our previous study (21), the challenge of A^+ macaques with a mutant SIVmac239 carrying GagL216S and GagD244E mutations showed higher set point viral loads, indicating that these A-derived, MHC-I-restricted, $Gag_{206-216}$ and $Gag_{241-249}$ epitope-specific $CD8^+$ T-cell responses are responsible for lower viral loads in group A^+ animals.

Our analysis revealed differences in the target antigens for predominant $CD8^+$ T-cell responses but not in the magnitudes of SIV-specific $CD8^+$ T-cell responses among four groups. However, we found differences in polyfunctional SIV-specific $CD4^+$ T-cell responses in the chronic phase. Remarkably, plasma viral loads inversely correlated with the polyfunctionality of SIV-specific $CD8^+$ T cells as well as $CD4^+$ T cells. These results suggest stronger polyfunctional T cell responses in animals with lower viral loads, which, conversely, could contribute to the sustained suppression of viral replication in the chronic phase.

In summary, we examined SIVmac239 infection in four groups of Burmese rhesus macaques, with each group sharing different MHC-I haplotypes. Our results indicate the association of MHC-I haplotypes with disease progression. This study presents a robust AIDS model of SIV infection facilitating the analysis of virus-host immune interaction.

ACKNOWLEDGMENTS

This work was supported by grants-in-aid from the Ministry of Education, Culture, Sports, Science, and Technology, grants-in-aid from the Ministry of Health, Labor, and Welfare, and a grant from Takeda Science Foundation in Japan.

The animal experiments were conducted through the Cooperative Research Program in Tsukuba Primate Research Center, National Institute of Biomedical Innovation, with the help of the Corporation for Production and Research of Laboratory Primates.

We thank F. Ono, K. Oto, A. Hiyaoka, K. Komatsuzaki, M. Hamano, Y. Emoto, H. Akari, and Y. Yasutomi for their assistance in animal experiments. We also thank M. Roederer for providing the PESTLE and SPICE software.

REFERENCES

1. **Alexander L, Denekamp L, Czajak S, Desrosiers RC.** 2001. Suboptimal nucleotides in the infectious, pathogenic simian immunodeficiency virus clone SIVmac239. J. Virol. 75:4019–4022.
2. **Almeida JR, et al.** 2007. Superior control of HIV-1 replication by CD8+ T cells is reflected by their avidity, polyfunctionality, and clonal turnover. J. Exp. Med. 204:2473–2485.
3. **Altfeld M, et al.** 2003. Influence of HLA-B57 on clinical presentation and viral control during acute HIV-1 infection. AIDS 17:2581–2591.
4. **Betts MR, et al.** 2006. HIV nonprogressors preferentially maintain highly functional HIV-specific CD8+ T cells. Blood 107:4781–4789.
5. **Bontrop RE, Watkins DI.** 2005. MHC polymorphism: AIDS susceptibility in non-human primates. Trends Immunol. 26:227–233.
6. **Borrow P, Lewicki H, Hahn BH, Shaw GM, Oldstone MB.** 1994. Virus-specific CD8+ cytotoxic T-lymphocyte activity associated with control of viremia in primary human immunodeficiency virus type 1 infection. J. Virol. 68:6103–6110.
7. **Boyson JE, et al.** 1996. The MHC class I genes of the rhesus monkey. Different evolutionary histories of MHC class I and II genes in primates. J. Immunol. 156:4656–4665.
8. **Carrington M, et al.** 1999. HLA and HIV-1: heterozygote advantage and B*35-Cw*04 disadvantage. Science 283:1748–1752.
9. **Daza-Vamenta R, Glusman G, Rowen L, Guthrie B, Geraghty DE.** 2004.

Genetic divergence of the rhesus macaque major histocompatibility complex. Genome Res. 14:1501–1515.
10. Evans DT, et al. 1999. Virus-specific cytotoxic T-lymphocyte responses select for amino-acid variation in simian immunodeficiency virus Env and Nef. Nat. Med. 5:1270–1276.
11. Evans DT, et al. 2000. Definition of five new simian immunodeficiency virus cytotoxic T-lymphocyte epitopes and their restricting major histocompatibility complex class I molecules: evidence for an influence on disease progression. J. Virol. 74:7400–7410.
12. Feinberg MB, Moore JP. 2002. AIDS vaccine models: challenging challenge viruses. Nat. Med. 8:207–210.
13. Goulder PJ, Watkins DI. 2004. HIV and SIV CTL escape: implications for vaccine design. Nat. Rev. Immunol. 4:630–640.
14. Goulder PJ, Watkins DI. 2008. Impact of MHC class I diversity on immune control of immunodeficiency virus replication. Nat. Rev. Immunol. 8:619–630.
15. Guidotti LG, Chisari FV. 2000. Cytokine-mediated control of viral infections. Virology 273:221–227.
16. Ishii H, et al. 2012. Impact of vaccination on cytotoxic T lymphocyte immunodominance and cooperation against simian immunodeficiency virus replication in rhesus macaques. J. Virol. 86:738–745.
17. Iwamoto N, et al. 2010. Broadening of CD8+ cell responses in vaccine-based simian immunodeficiency virus controllers. AIDS 24:2777–2787.
18. Jin X, et al. 1999. Dramatic rise in plasma viremia after CD8(+) T cell depletion in simian immunodeficiency virus-infected macaques. J. Exp. Med. 189:991–998.
19. Kawada M, et al. 2006. Involvement of multiple epitope-specific cytotoxic T-lymphocyte responses in vaccine-based control of simian immunodeficiency virus replication in rhesus macaques. J. Virol. 80:1949–1958.
20. Kawada M, et al. 2007. Long-term control of simian immunodeficiency virus replication with central memory CD4+ T-cell preservation after nonsterile protection by a cytotoxic T-lymphocyte-based vaccine. J. Virol. 81:5202–5211.
21. Kawada M, et al. 2008. Gag-specific cytotoxic T-lymphocyte-based control of primary simian immunodeficiency virus replication in a vaccine trial. J. Virol. 82:10199–10206.
22. Kestler HW, III, et al. 1991. Importance of the nef gene for maintenance of high virus loads and for development of AIDS. Cell 65:651–662.
23. Kiepiela P, et al. 2004. Dominant influence of HLA-B in mediating the potential co-evolution of HIV and HLA. Nature 432:769–775.
24. Kiepiela P, et al. 2007. CD8+ T-cell responses to different HIV proteins have discordant associations with viral load. Nat. Med. 13:46–53.
25. Koup RA, et al. 1994. Temporal association of cellular immune responses with the initial control of viremia in primary human immunodeficiency virus type 1 syndrome. J. Virol. 68:4650–4655.
26. Kulski JK, Anzai T, Shiina T, Inoko H. 2004. Rhesus macaque class I duplicon structures, organization and evolution within the alpha block of the major histocompatibility complex. Mol. Biol. Evol. 21:2079–2091.
27. Leslie A, et al. 2010. Additive contribution of HLA class I alleles in the immune control of HIV-1 infection. J. Virol. 84:9879–9888.
28. Letvin NL, et al. 2006. Preserved CD4+ central memory T cells and survival in vaccinated SIV-challenged monkeys. Science 312:1530–1533.
29. Loffredo JT, et al. 2008. Patterns of CD8+ immunodominance may influence the ability of Mamu-B*08-positive macaques to naturally control simian immunodeficiency virus SIVmac239 replication. J. Virol. 82: 1723–1738.
30. Loffredo JT, et al. 2007. Mamu-B*08-positive macaques control simian immunodeficiency virus replication. J. Virol. 81:8827–8832.
31. Matano T, et al. 2004. Cytotoxic T lymphocyte-based control of simian immunodeficiency virus replication in a preclinical AIDS vaccine trial. J. Exp. Med. 199:1709–1718.
32. Matano T, et al. 1998. Administration of an anti-CD8 monoclonal antibody interferes with the clearance of chimeric simian/human immunodeficiency virus during primary infections of rhesus macaques. J. Virol. 72: 164–169.
33. Migueles SA, et al. 2000. HLA B*5701 is highly associated with restriction of virus replication in a subgroup of HIV-infected long term nonprogressors. Proc. Natl. Acad. Sci. U. S. A. 97:2709–2714.
34. Miura T, et al. 2009. HLA-B57/B*5801 human immunodeficiency virus type 1 elite controllers select for rare gag variants associated with reduced viral replication capacity and strong cytotoxic T-lymphocyte recognition. J. Virol. 83:2743–2755.
35. Morgan C, et al. 2008. The use of nonhuman primate models in HIV vaccine development. PLoS Med. 5:e173.
36. Mothe BR, et al. 2003. Expression of the major histocompatibility complex class I molecule Mamu-A*01 is associated with control of simian immunodeficiency virus SIVmac239 replication. J. Virol. 77:2736–2740.
37. Muhl T, Krawczak M, Ten Haaft P, Hunsmann G, Sauermann U. 2002. MHC class I alleles influence set-point viral load and survival time in simian immunodeficiency virus-infected rhesus monkeys. J. Immunol. 169:3438–3446.
38. Naruse TK, et al. 2010. Diversity of MHC class I genes in Burmese-origin rhesus macaques. Immunogenetics 62:601–611.
39. O'Connor DH, et al. 2002. Acute phase cytotoxic T lymphocyte escape is a hallmark of simian immunodeficiency virus infection. Nat. Med. 8:493–499.
40. O'Connor SL, et al. 2010. MHC heterozygote advantage in simian immunodeficiency virus-infected Mauritian cynomolgus macaques. Sci. Transl. Med. 2:22ra18.
41. Otting N, et al. 2005. Unparalleled complexity of the MHC class I region in rhesus macaques. Proc. Natl. Acad. Sci. U. S. A. 102:1626–1631.
42. Roederer M, Nozzi JL, Nason MC. 2011. SPICE: exploration and analysis of post-cytometric complex multivariate datasets. Cytometry A 79:167–174.
43. Schmitz JE, et al. 1999. Control of viremia in simian immunodeficiency virus infection by CD8+ lymphocytes. Science 283:857–860.
44. Seder RA, Hill AV. 2000. Vaccines against intracellular infections requiring cellular immunity. Nature 406:793–798.
45. Seder RA, Darrah PA, Roederer M. 2008. T-cell quality in memory and protection: implications for vaccine design. Nat. Rev. Immunol. 8:247–258.
46. Shibata R, et al. 1997. Infection and pathogenicity of chimeric simian-human immunodeficiency viruses in macaques: determinants of high virus loads and CD4 cell killing. J. Infect. Dis. 176:362–373.
47. Sodora DL, et al. 2009. Toward an AIDS vaccine: lessons from natural simian immunodeficiency virus infections of African nonhuman primate hosts. Nat. Med. 15:861–865.
48. Stinchcombe JC, Bossi G, Booth S, Griffiths GM. 2001. The immunological synapse of CTL contains a secretory domain and membrane bridges. Immunity 15:751–761.
49. Takahara Y, et al. 2011. Dominant induction of vaccine antigen-specific cytotoxic T lymphocyte responses after simian immunodeficiency virus challenge. Biochem. Biophys. Res. Commun. 408:615–619.
50. Tanaka-Takahashi Y, et al. 2007. Reference strand-mediated conformation analysis-based typing of multiple alleles in the rhesus macaque MHC class I Mamu-A and Mamu-B loci. Electrophoresis 28:918–924.
51. Tang J, et al. 2002. Favorable and unfavorable HLA class I alleles and haplotypes in Zambians predominantly infected with clade C human immunodeficiency virus type 1. J. Virol. 76:8276–8284.
52. Tenzer S, et al. 2009. Antigen processing influences HIV-specific cytotoxic T lymphocyte immunodominance. Nat. Immunol. 10:636–646.
53. Tsukamoto T, et al. 2009. Impact of cytotoxic-T-lymphocyte memory induction without virus-specific CD4+ T-cell help on control of a simian immunodeficiency virus challenge in rhesus macaques. J. Virol. 83:9339–9346.
54. Wang YE, et al. 2009. Protective HLA class I alleles that restrict acute-phase CD8+ T-cell responses are associated with viral escape mutations located in highly conserved regions of human immunodeficiency virus type 1. J. Virol. 83:1845–1855.
55. Wilson NA, et al. 2006. Vaccine-induced cellular immune responses reduce plasma viral concentrations after repeated low-dose challenge with pathogenic simian immunodeficiency virus SIVmac239. J. Virol. 80:5875–5885.
56. Wiseman RW, et al. 2007. Simian immunodeficiency virus SIVmac239 infection of major histocompatibility complex-identical cynomolgus macaques from Mauritius. J. Virol. 81:349–361.
57. Yamamoto H, Kawada M, Takeda A, Igarashi H, Matano T. 2007. Post-infection immunodeficiency virus control by neutralizing antibodies. PLoS One 2:e540.
58. Yamamoto T, et al. 2009. Polyfunctional CD4+ T-cell induction in neutralizing antibody-triggered control of simian immunodeficiency virus infection. J. Virol. 83:5514–5524.
59. Yant LJ, et al. 2006. The high-frequency major histocompatibility complex class I allele Mamu-B*17 is associated with control of simian immunodeficiency virus SIVmac239 replication. J. Virol. 80:5074–5077.

RETROVIROLOGY

RESEARCH Open Access

Quantification system for the viral dynamics of a highly pathogenic simian/human immunodeficiency virus based on an *in vitro* experiment and a mathematical model

Shingo Iwami[1,2,3,6*], Benjamin P Holder[4], Catherine AA Beauchemin[4], Satoru Morita[5], Tetsuko Tada[3], Kei Sato[3], Tatsuhiko Igarashi[3] and Tomoyuki Miura[3*]

Abstract

Background: Developing a quantitative understanding of viral kinetics is useful for determining the pathogenesis and transmissibility of the virus, predicting the course of disease, and evaluating the effects of antiviral therapy. The availability of data in clinical, animal, and cell culture studies, however, has been quite limited. Many studies of virus infection kinetics have been based solely on measures of total or infectious virus count. Here, we introduce a new mathematical model which tracks both infectious and total viral load, as well as the fraction of infected and uninfected cells within a cell culture, and apply it to analyze time-course data of an SHIV infection *in vitro*.

Results: We infected HSC-F cells with SHIV-KS661 and measured the concentration of Nef-negative (target) and Nef-positive (infected) HSC-F cells, the total viral load, and the infectious viral load daily for nine days. The experiments were repeated at four different MOIs, and the model was fitted to the full dataset simultaneously. Our analysis allowed us to extract an infected cell half-life of 14.1 h, a half-life of SHIV-KS661 infectiousness of 17.9 h, a virus burst size of 22.1 thousand RNA copies or 0.19 $TCID_{50}$, and a basic reproductive number of 62.8. Furthermore, we calculated that SHIV-KS661 virus-infected cells produce at least 1 infectious virion for every 350 virions produced.

Conclusions: Our method, combining *in vitro* experiments and a mathematical model, provides detailed quantitative insights into the kinetics of the SHIV infection which could be used to significantly improve the understanding of SHIV and HIV-1 pathogenesis. The method could also be applied to other viral infections and used to improve the *in vitro* determination of the effect and efficacy of antiviral compounds.

Keywords: Viral infectiousness, Quantification of viral dynamics, *In vitro* experiment, Mathematical model, Simian/Human immunodeficiency virus

Background

Historically, the study of the highly pathogenic simian/human immunodeficiency virus (SHIV) has provided important information for the understanding of human immunodeficiency virus type-1 (HIV-1) pathogenesis. For example, it was clarified in an SHIV animal study that co-receptor usage determined by the HIV-1 *env* gene affects the virus' cell tropism (preference for specific target cell populations), and thus its pathogenesis, *in vivo* [1-3]. Furthermore, infections with highly pathogenic SHIV strains in animal models have exhibited stable clinical manifestations in most infected animals, similar to an aspect of infection course in human HIV infections [4,5]. One of the highly pathogenic SHIV strains, SHIV-KS661, which has the *env* gene of HIV-1 89.6 and predominantly uses CXCR4 as the secondary receptor for its infection [2], causes an infection that

* Correspondence: siwami@ms.u-tokyo.ac.jp; tmiura@virus.kyoto-u.ac.jp
[1]Precursory Research for Embryonic Science and Technology (PRESTO), Japan Science and Technology Agency (JST), Kawaguchi, Saitama 332-0012, Japan
[3]Institute for Virus Research, Kyoto University, Kyoto, Kyoto 606-8507, Japan
Full list of author information is available at the end of the article

systemically depletes the $CD4^+$ T cells of rhesus macaques within 4 weeks after infection [6,7]. In observations by our group in recent years, the intravenous infection of rhesus macaques with SHIV-KS661 has consistently resulted in high viremia and $CD4^+$ T cell depletion, followed by malignant morbidity as a result of severe chronic diarrhea and wasting after 6 to 18 months [8]. Despite this well-developed *in vivo* model, the detailed kinetics of SHIV-KS661 remain unclear. Quantifying and understanding viral kinetics will provide us with novel insights about the pathogenesis of SHIV (and HIV-1), for example, by enabling the quantitative comparison of the replicative capacity of different strains.

In recent years, virological data from clinical patient studies, animal experiments, and cell culture studies have frequently been analyzed using mathematical models. Mathematical analysis of clinical data is an increasingly popular tool for the evaluation of drugs, the elaboration of diagnostic criteria, and the generation of recommendations for effective therapies [9-17]. Analyses of animal and cell culture studies have revealed fundamental aspects of viral infections including the specification of the half-life of infected cells and virus, the virus burst size, and the relative contribution of the immune response [18-29]. Important results have also been obtained in the analysis of purely *in vitro* experiments. For example, in Beauchemin *et. al.* [19], simple mathematical models were employed to analyze the effect of amantadine treatment on the course of experimental infections of Madin Darby canine kidney (MDCK) cells with influenza A/Albany/1/98 (H3N2) in a hollow-fiber (HF) reactor. Fits of the models to the experimental data determined that the 50% inhibitory concentration (IC_{50}) of amantadine for that particular strain was 0.3-0.4 μM and found amantadine to be 56-74% effective at blocking the infection of target cells. Thus, analyses of experimental data using mathematical models have provided, and continue to provide, quantitative information about the kinetics of viral infections - particularly for HIV-1, the hepatitis C virus (HCV), and the influenza virus - by estimating infection parameters buried within experimental data.

Despite these successes, the available virological data, even for *in vitro* experiments, have often been limited in that many modeling analyses have been based only on total viral load data (e.g., RNA or DNA copies, hemagglutination assay (HA)) [9-13,15-17,20,22,23,26,27] or infectious viral load data (e.g., 50% tissue culture infection dose ($TCID_{50}$) or plaque forming units (PFU)) [18,19,25]. Thus, while the applied mathematical models typically depend on the interaction of many components of the infection - including the populations of susceptible and infected cells - they are often only confronted by a single biological quantity: the time-course of the viral load. More rarely, diverse data sets including both virus and cell measurements have been considered [14,29-37]. Notable examples of the latter case include the analysis of an influenza infection in a microcarrier culture by Schulz-Horsel *et al.* [29], who measured and modeled the infectious and total viral load, along with the fraction of infected cells; and the *in vivo* studies of HIV-1 dynamics following antiviral therapy by Perelson and co-workers (e.g., [14,31]), who have considered measurements of viral load as well as susceptible and infected cells.

Here, we combined a relatively simple mathematical model of SHIV infection in HSC-F cells with an *in vitro* experimental system which allows for the measurement of both total and infectious viral load and the concentration of target and infected cells. We infected HSC-F - a $CD4^+$ T cell line established from cynomolgus monkey - *in vitro* with SHIV-KS661 at four different multiplicities of infection (MOI) and measured the concentration of Nef-negative (susceptible/target) and Nef-positive (infected/virus producing) HSC-F cells [cells/ml], and the total [RNA copies/ml] and infectious [$TCID_{50}$/ml] viral load daily over nine days. With this abundant and diverse data, we were able to fully parameterize the dynamic model and determine robust estimates for viral kinetics parameters, thus quantifying the infection cycle. Our *in vitro* quantification system for SHIV-KS661 should be a valuable complement to the well-developed *in vivo* model and can be used to significantly improve the understanding of SHIV and HIV-1 pathogenesis.

Results

Mathematical model

To describe the *in vitro* kinetics of the SHIV-KS661 viral infection in our experimental system (Table 1), we expanded a basic mathematical model widely used for analyzing viral kinetics [13,17-19,27,38,39]. The following equations are our extended model:

$$\frac{dx}{dt} = -\beta x v_I - dx \tag{1}$$

$$\frac{dy}{dt} = \beta x v_I - ay \tag{2}$$

$$\frac{dv_I}{dt} = pky - r_I v_I - r_{RNA} v_I \tag{3}$$

$$\frac{dv_{NI}}{dt} = (1-p)ky + r_I v_I - r_{RNA} v_{NI} \tag{4}$$

where x and y are the number of target (susceptible) and infected (virus-producing) cells per ml of medium,

Table 1 Experimental data for the *in vitro* experiment

MOI	Measurement day								
	0	1	2	3	4	5	6	7	8
Concentration of Nef-negative HSC-F cells (cells/ml)									
2×10^{-3}	5470829	6044623	2690861	1012828	223584	42130	58470	10386	10270
2×10^{-4}	2333804	4953074	2985268	2201172	811240	621750	60255	19998	4857
2×10^{-5}	2574201	3563431	3434160	2345412	1269216	1345728	264794	71792	127996
2×10^{-6}	3357117	2583058	4557411	35074989	1334060	1896048	1022157	307908	153360
Concentration of Nef-positive HSC-F cells (cells/ml)									
2×10^{-3}	d.l.*	d.l.	439139	1167172	736416	177870	41530	19614	9730
2×10^{-4}	d.l.	d.l.	84732	158828	548760	878250	89745	40002	5143
2×10^{-5}	d.l.	d.l.	d.l.	64588	170784	574272	165206	88208	92004
2×10^{-6}	d.l.	d.l.	d.l.	d.l.	65940	383952	347843	232092	86640
Total viral load of SHIV-KS661 (RNA copies/ml)									
2×10^{-3}	9180000	331000000	2840000000	4050000000	3140000000	1120000000	154000000	20200000	5650000
2×10^{-4}	1030000	26200000	256000000	1670000000	2110000000	1740000000	609000000	134000000	19400000
2×10^{-5}	126744	4370000	51200000	489000000	1280000000	1940000000	1230000000	570000000	130000000
2×10^{-6}	10170	800536	4600000	54200000	322000000	1300000000	1210000000	603000000	275000000
Infectious viral load of SHIV-KS661 ($TCID_{50}$/ml)									
2×10^{-3}	40	4064	40960	81920	163840	20480	2560	160	d.l.
2×10^{-4}	d.l.	101	403	5120	16255	40960	1280	101	40
2×10^{-5}	d.l.	64	640	4064	20480	25803	5120	1280	640
2×10^{-6}	40	40	80	640	5120	1280	1280	640	1280

"d.l." designates samples in which the concentration was below the detection limit.

v_I and v_{NI} are the number of RNA copies of infectious and non-infectious virus per ml of medium, respectively. Parameters d, a, r_{RNA}, and β represent the death rate of target cells, the death rate of infected cells, the degradation rate of viral RNA, and the rate constant for infection of target cells by virus, respectively. We assume that each infected cell releases k virus particles per day (i.e., k is the viral production rate of an infected cell), of which a fraction p are infectious and $1\text{-}p$ are non-infectious. Infectious virions lose infectivity at rate r_I, becoming non-infectious. Implicit in Eqs.(1)-(4) is the assumption that once a cell is infected by infectious virus it immediately begins producing progeny virus. We also tested a variant of the model which incorporates an "eclipse" phase of infection to represent the cell's period of latency prior to virus production. We found, however, that including this phase did not significantly improve the fit of the model to the data and led to very similar extracted parameter values (see Additional files 1, 2, 3). Therefore, in all further analyses, this phase was omitted in favor of the simpler model formulation. A schematic of our mathematical model is shown in Figure 1.

To fit the observed viral load data - consisting of RNA copies/ml and $TCID_{50}$/ml - and to account for the partial removal of cells and virus due to sampling, we transformed Eqs.(1)-(4) into the following scaled model:

$$\frac{dx}{dt} = -\beta_{50} x v_{50} - dx - \delta x \tag{5}$$

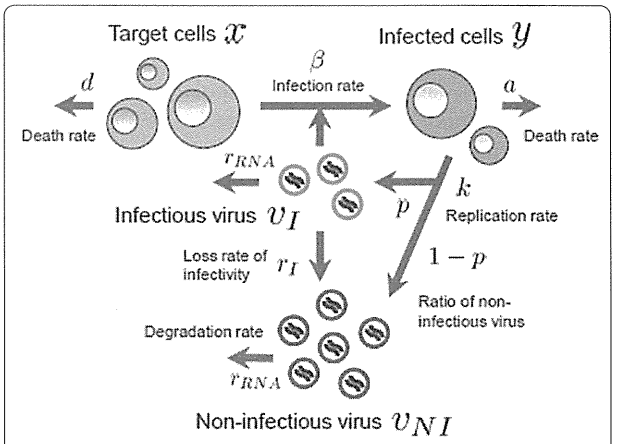

Figure 1 A schematic representation of the mathematical model. The variables x and y are the number of target and infected cells; v_I and v_{NI} are the number of RNA copies of infectious and non-infectious virus, respectively. Parameters d, a, r_{RNA}, and β represent the death rate of target cells, the death rate of infected cells, the degradation rate of viral RNA, and the rate constant for infection of cells by infectious virus, respectively. It is assumed that infected cells release virus particles at a rate k, that a fraction p of these particles are infectious ($1\text{-}p$ are non-infectious) but lose infectivity at a rate r_I, becoming non-infectious.

$$\frac{dy}{dt} = \beta_{50} x v_{50} - a y - \delta y \quad (6)$$

$$\frac{dv_{RNA}}{dt} = k y - r_{RNA} v_{RNA} - r_c v_{RNA} \quad (7)$$

$$\frac{dv_{50}}{dt} = k_{50} y - r_I v_{50} - r_{RNA} v_{50} - r_c v_{50} \quad (8)$$

where $v_{RNA} = v_I + v_{NI}$ is the total concentration of viral RNA copies, $v_{50} = \alpha v_I$ is the infectious viral load expressed in $TCID_{50}$/ml, and α is the conversion factor from infectious viral RNA copies to $TCID_{50}$. Since the measure of 1 $TCID_{50}$ corresponds to an average of 0.68 infection events (by Poisson statistics), we have $0 < \alpha \leqq 1.47$ $TCID_{50}$ per RNA copies of infectious virus. Parameters $\beta_{50} = \beta/\alpha$ and $k_{50} = \alpha pk$ are the converted infection rate constant and production rate of infectious virus, respectively. At each sampling time, the concentration of Nef-negative and Nef-positive HSC-F cells must be reduced in our model by 5.5% and the viral loads (RNA copies and $TCID_{50}$) by 99.93% to account for the experimental harvesting of cells and virus. These losses were modeled in Eqs.(5)-(8) by approximating the sampling of cells and virus as a continuous exponential decay, yielding a rate of $\delta = 0.057$ per day for cell harvest and $r_c = 7.31$ per day for virus harvest. We found that a model which implements the sampling explicitly, as a punctual reduction at each sampling time, similar to the model in [19], did not significantly improve the quality of the fit (data not shown).

Of the seven free model parameters remaining, three of them (d, r_I, r_{RNA}) were determined by direct measurements in separate experiments described below. The remaining four parameters (β_{50}, a, k, k_{50}) along with 16 initial ($t = 0$) values for the variables (four at each of the four MOI values) were determined by fitting the model to the data as described in **Methods** (Tables 2 and 3).

In vitro half-lives of the SHIV-KS661 virus and HSC-F cells

The rates at which SHIV-KS661 virions lose infectivity, r_I, and the rate at which their viral RNA degrades, r_{RNA}, were each estimated directly in separate experiments (Figure 2). Linear regressions were performed to fit $logv_{RNA}(t) = logv_{RNA}(0) - r_{RNA}t$ and $logv_{50}(t) = logv_{50}(0) - r_I t$ to those data, yielding values of $r_{RNA} = 0.039$ per day (95% confidence interval (95%CI): *0.013-0.065* per day) and $r_I = 0.93$ per day (95%CI: *0.44-1.4* per day). These correspond to an infectious virion half-life of *17.9* h and an RNA viability half-life of *17.7* d. The death rate of target cells, d, was also estimated directly, in a mock infection experiment where Nef-negative (target) HSC-F cells were exposed to the culture conditions of the experiment without virus (data not shown). A linear regression was performed to fit $logx(t) = logx(0) - (d+\delta)t$ to the time course data, yielding $d = 0.21$ per day (95% CI: *0.18-0.27*), corresponding to an average target cell lifespan of *4.76* d (half-life of *3.30* d).

Time-course *in vitro* data

Time-course *in vitro* experimental data were collected over nine days, consisting of the concentrations of Nef-

Table 2 Parameters values and derived quantities for the *in vitro* experiment

Parameter Name	Symbol	Unit	Value	95%CI
Calculated parameters for the continuous approximation of cell and virus harvest				
Harvest rate of target and infected cells	δ	day^{-1}	0.057	-
Harvest rate of total and infectious virus	r_c	day^{-1}	7.31	-
Fitted parameters from separate experiments				
Decay rate of uninfected cells	d	day^{-1}	0.21	0.17-0.26
Rate of virion infectivity loss	r_I	day^{-1}	0.93	0.44-1.4
Degradation rate of virion RNA	r_{RNA}	day^{-1}	0.039	0.013-0.065
Parameters obtained from simultaneous fit to full *in vitro* dataset				
Rate constant for infections	β_{50}	$(TCID_{50}/ml \cdot day)^{-1}$	4.95×10^{-5}	$(2.35\text{-}9.59) \times 10^{-5}$
Decay rate of infected cells	a	day^{-1}	1.18	0.85-1.26
Production rate of total virus	k	RNA copies·day^{-1}	2.61×10^{4}	$(1.55\text{-}3.70) \times 10^{4}$
Production rate of infectious virus	k_{50}	$TCID_{50} \cdot day^{-1}$	0.22	0.12-0.40
Quantities derived from fitted values				
Viral burst size (total)	k/a	RNA copies	2.21×10^{4}	$(1.74\text{-}2.96) \times 10^{4}$
Viral burst size (infectious)	k_{50}/a	$TCID_{50}$	0.19	0.11-0.33
Basic reproductive number (without removal)	R_0	-	62.8	51.1-76.8
Basic reproductive number (with removal)	R_0*	-	7.01	5.70-8.45
Minimum fraction of infectious virus	k_{50}/k	$TCID_{50}$/RNA copies	8.63×10^{-6}	$(4.53\text{-}16.9) \times 10^{-6}$

Table 3 Fitted initial (t = 0) values for the *in vitro* experiment

Variable	Unit	Fitted initial value at MOI of			
		2×10^{-3}	2×10^{-4}	2×10^{-5}	2×10^{-6}
$x_j(0)$	cells/ml	6.55×10^6	6.50×10^6	5.82×10^6	4.94×10^6
$y_j(0)$	cells/ml	6.47×10^2	1.60×10^2	6.89×10^{-3}	0.254
$v_{RNAj}(0)$	RNA copies/ml	9.15×10^6	1.05×10^6	1.58×10^5	8.21×10^3
$v_{50j}(0)$	$TCID_{50}$/ml	43.1	0.162	2.92	2.99

negative and Nef-positive HSC-F cells [cells/ml], the total SHIV-KS661 viral load [RNA copies/ml], and the infectious viral load [$TCID_{50}$/ml]. At each daily measurement, almost all of the culture supernatant (99.93%) was removed for viral counting; a small percentage of cells (5.5%) were removed for counting and FACS analysis, and the remaining cells were thoroughly washed and replaced in fresh medium. The experiment was repeated for four different values of the initial viral inoculum (MOI). In total, we obtained 130 data points for quantifying SHIV-KS661 viral kinetics *in vitro* (Table 1 **and** Figure 3).

In examining the MOI = 2×10^{-3} data, one can see that the target cell population remains high (near its initial value of approximately 6.46×10^6 cells/ml) until just before the peak of the virus concentration, at which point the target cell population decreases rapidly. The total infected cell population, the total virus count (RNA/ml), and the infectious virus count ($TCID_{50}$/ml) all peak around $t = 3$ days. Moreover, the rate of exponential decay (downward slope) of the total virus and the infected cell population after their respective peaks are quite similar. This behavior is expected: since the virus is being almost completely removed from the culture on a daily basis due to sampling and the RNA degradation rate is very small ($r_{RNA} = 0.039$ per day); the measured RNA count of virus is nearly equal to the total number of virus produced over the preceding day which should be proportional to the number of cells producing virus. Similar reasoning should apply to the decay of infectious virus - the net infectious virus measured after one day should also be approximately proportional to the number of infected cells - but the rates appear much less closely aligned in this case, perhaps due to larger errors in the $TCID_{50}$ measurement technique. Alternatively, the observed more rapid than expected decrease of infectious virus could have a biological cause. For instance, the co-infection of cells by competent and defective interfering viruses at late stages in the experiment could lead to an enhanced production of the latter [40], thus successively reducing the fraction of infectious particles. An increase in cell-death by-products could also contribute to the decline in virus infectivity. In SIV and SHIV infections *in vivo*, a decreasing viral infectiousness has been observed over time

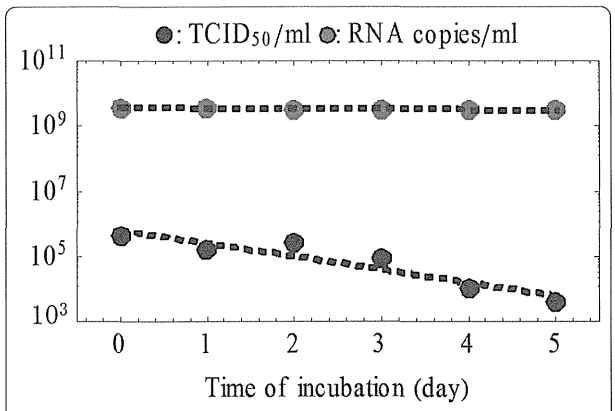

Figure 2 Rates of RNA degradation and loss of infectivity for SHIV-KS661. Stock virus was incubated under the same conditions as the infection experiments, but in the absence of cells, then sampled every day and stored at -80°C. After the sampling, the RNA copy number (gray circles) and 50% tissue culture infectious dose (black circles) of the samples were measured. Linear regressions yielded a rate of RNA degradation of $r_{RNA} = 0.039$ per day and a rate of loss of viral infectivity of $r_I = 0.93$ per day.

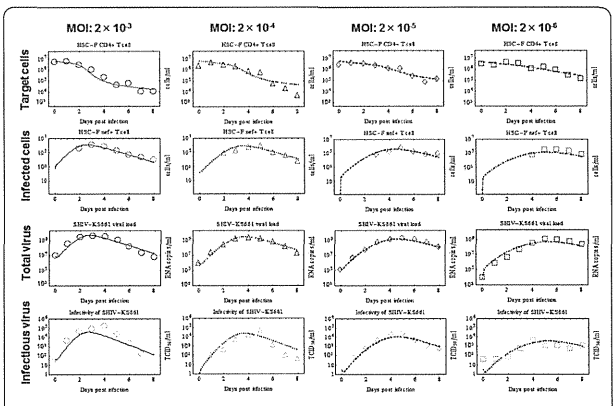

Figure 3 Fits of the mathematical model to experimental data of SHIV-KS661 *in vitro*. HSC-F cells were inoculated with SHIV-KS661 24 h before $t = 0$, and each *in vitro* experimental quantity was measured daily from $t = 0$ d to 8 d. The curves show the best-fit of the model (Eqs.(5)-(8), lines) to the experimental data (points) for the target cells, infected cells, and the total and infectious viral load for the four different experiments conducted at different MOIs. All data were fitted simultaneously as described in the text. The fitted $t = 0$ values of each quantity are given in **Table 3**.

[7,41,42], but the timescale of this decay is longer than that observed here and likely has an in-host origin.

A comparison of the experiments at the four different MOI values shows that a decrease in the initial viral inoculum serves primarily to delay the course of the infection. The target cell populations drop to approximately half of their original values at $t \approx 1.9, 2.6, 3.5$ and 4.1 days, respectively, for the four experiments in order of decreasing MOI. Similarly the peaks of the total viral RNA occur at $t \approx 3.0, 4.0, 5.0$ and 5.5 days, respectively. The experiments at lower MOI have slightly lower viral and infected cell peaks, but differ from those of the experiment at MOI = 2×10^{-3} by less than a factor of three.

Relevant SHIV-KS661 viral kinetics measures

Having fixed the values of the rates of virion decay (r_I and r_{RNA}) and the target cell death rate (d) using separate experiments, we estimated the values and 95% CI of the four remaining unknown parameters (β_{50}, a, k, k_{50}) by fitting the model in Eqs.(5)-(8) to the full *in vitro* dataset simultaneously (Table 2). The death rate of infected cells was determined to be $a = 1.18$ per day (95%CI: *0.85-1.26* per day) which implies that the half-life of infected cells (i.e., $log2/a$) is *14.1* h. Infected HSC-F cells were found to produce $k = 2.61 \times 10^4$ RNA copies of virus per day.

From the directly fitted parameters, we also calculated a number of important derived quantities and their 95% CI, determined from the bootstrap fits (Table 2). One key measurement of viral kinetics is the viral burst size, which is the total number of virus produced by an infected cell during its lifetime [18-20]. The total burst size of SHIV-KS661 (including non-infectious and infectious virus) is given in our model by k/a and was estimated from our *in vitro* experiment to be 2.21×10^4 RNA copies. The burst size of infectious SHIV-KS661, k_{50}/a, was *0.19* $TCID_{50}$.

To broadly characterize viral kinetics, it is instructive to calculate the basic reproductive number for the system, which has the form $R_0 = \beta_{50}k_{50}x_0/(a(r_I+r_{RNA}))$ and is interpreted as the number of newly infected cells intrinsically generated by a single infectious cell at the start of the infection [15-19,27]. The initial number of HSC-F cells, x_0, was approximately 6.46×10^6 cells/ml, which, together with the values of the five estimated parameters, yields an estimate for the basic reproductive number of *62.8*. This large value ($62.8 \gg 1$) implies that, given a small initiating infected cell population, the infection is overwhelmingly likely to spread to the entire population of cells.

After the repetitive removal of cells and virus begins, the basic reproductive number is effectively reduced, much like the effect of quarantine on the epidemiological measure of R_0. When the effects of removal are included in the calculation of the basic reproductive number it has the form $R_0^* = \beta_{50}k_{50}x_0/((a+\delta)(r_I+r_{RNA}+r_C))$ which yields a smaller value of 7.01. This value better characterizes the course of the infection in our system, for example, through the recursive relation for the approximate fraction of eventually infected cells, $f_I = 1- exp(-R_0^* f_I)$ [43]. Using this expression, we find that the fraction of target cells at the end of the infection ($1-f_I$) should be 9.01×10^{-4}, which implies an approximately final target cell concentration is 5.87×10^3 cells/ml. This value agrees well with the asymptotic concentration of Nef-negative HSC-F cells in the MOI = 2×10^{-3} experiment, $\sim 1.03 \times 10^4$ cells/ml. The delay of the infection precludes an estimate of the final target cell value at smaller MOI values.

Our model formulation also enables us to determine, albiet not fully, two interesting quantities related to the infectiousness of SHIV-KS66 virions. Parameter p (where $0 < p \leqq 1$) is the fraction of SHIV-KS66 virions which are infectious at the time of production: the larger the value of p, the fewer defective virus particles are produced by infectious cells. Parameter α is approximately the fraction of infectious virions which are measured in the $TCID_{50}$ assay, i.e., it is the ratio of $TCID_{50}$ viral titer (v_{50}) to the RNA count of infectious virions (v_I). It follows from Poisson statistics that $0 < \alpha \leqq 1.47$ $TCID_{50}$ per infectious RNA copies of infectious virions. While we cannot determine p and α individually in our analysis, their product is given by $k_{50}/k = (\alpha pk)/k = \alpha p = 8.63 \times 10^{-6}$ $TCID_{50}$ per infectious RNA copies. Because of the upper bounds on p and α, the value of their product imposes a minimum condition on each: $5.87 \times 10^{-6} < p \leqq 1$ and $8.63 \times 10^{-6} < \alpha \leqq 1.47$ $TCID_{50}$ per RNA copies.

We can constrain these parameters further by considering the basic reproductive number $R_0 = 62.8$, which implies that one infectious cell will infect *62.8* other cells over the course of its infectious lifespan. Thus, one infectious cell must produce at least *62.8* infectious virions over its lifespan, i.e., have a burst size of at least *62.8* infectious RNA copies. The burst size in infectious virions is given by pk/a, so this requirement can be written as $pk/a \geq R_0$ infectious RNA copies (or, equivalently, $p \geq aR_0/k$ infectious RNA copies) which, based on the values of these quantities from Table 2 implies that $p \geq 2.84 \times 10^{-3}$. Thus $2.84 \times 10^{-3} \leqq p \leqq 1$, which means that at least one in every 350 virions produced is infectious. Since $\alpha p = 8.63 \times 10^{-6}$ $TCID_{50}$ per infectious RNA copies, it follows that $8.63 \times 10^{-6} < \alpha \leqq 3.04 \times 10^{-3}$ $TCID_{50}$ per infectious RNA copies, which means that 1 $TCID_{50}$ corresponds to at least *330* ($1/3.04 \times 10^{-3}$) infectious virus, but perhaps as many as *120, 000* ($1/8.63 \times 10^{-6}$).